cmgh
CELLULAR AND MOLECULAR GASTROENTEROLOGY AND HEPATOLOGY

ORIGINAL RESEARCH

PHLDB2 Mediates Cetuximab Resistance via Interacting With EGFR in Latent Metastasis of Colorectal Cancer

Maochao Luo,[1,2,*] Zhao Huang,[1,2,*] Xingyue Yang,[1,2,*] Yan Chen,[1,2,*] Jingwen Jiang,[1,2] Lu Zhang,[1,2] Li Zhou,[1,2] Siyuan Qin,[1,2] Ping Jin,[1,2] Shuyue Fu,[1,2] Liyuan Peng,[1,2] Bowen Li,[1,2] Yongting Fang,[1,2] Wenchen Pu,[1] Yanqiu Gong,[1] Yu Liu,[1] Zhixiang Ren,[1] Qiu-Luo Liu,[3] Cun Wang,[3] Fangqiong Xiao,[2] Du He,[4] Hongying Zhang,[4] Changlong Li,[2] Heng Xu,[1] Lunzhi Dai,[1] Yong Peng,[1] Zong-Gung Zhou,[3] Canhua Huang,[1,2] and Hai-Ning Chen[3]

[1]State Key Laboratory of Biotherapy and Cancer Center, West China Hospital, Sichuan University, and Collaborative Innovation Center for Biotherapy, Chengdu, China; [2]West China School of Basic Medical Sciences & Forensic Medicine, Sichuan University, Chengdu, China; [3]Department of Gastrointestinal Surgery, State Key Laboratory of Biotherapy and Cancer Center, West China Hospital, Sichuan University, Chengdu, China; and [4]Department of Pathology, West China Hospital, Sichuan University, Chengdu, China

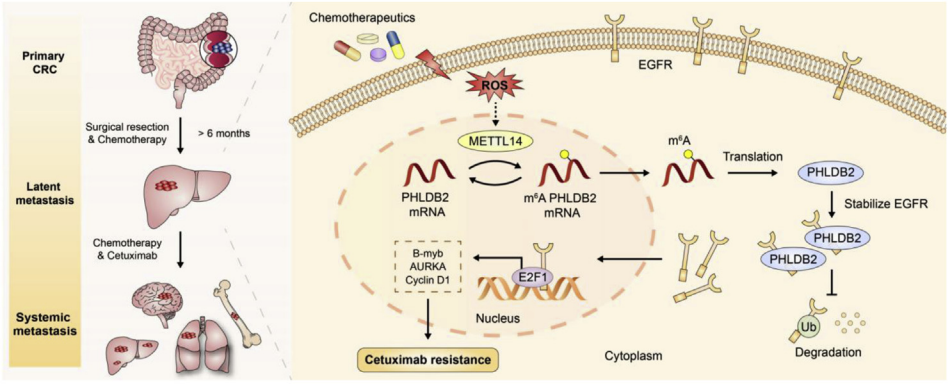

SUMMARY

Pleckstrin homology-like domain, family B, member 2 (PHLDB2) is up-regulated by chemotherapeutic agent–induced oxidative stress in latent liver metastasis of colorectal cancer. Moreover, up-regulated PHLDB2 stabilizes epidermal growth factor receptor and promotes its nuclear translocation, resulting in epidermal growth factor receptor signaling activation and cetuximab resistance.

BACKGROUND & AIMS: Latent metastasis of colorectal cancer (CRC) frequently develops months or years after primary surgery, followed by adjuvant therapies, and may progress rapidly even with targeted therapy administered, but the underlying mechanism remains unclear. Here, we aim to explore the molecular basis for the aggressive behavior of latent metastasis in CRC.

METHODS: Transcriptional profiling and pathway enrichment analysis of paired primary and metastatic tumor samples were performed. The underlying mechanisms of pleckstrin homology-like domain, family B, member 2 (PHLDB2) in CRC were investigated by RNA immunoprecipitation assay, immunohistochemistry, mass spectrometry analysis, and Duolink in situ proximity ligation assay (Sigma-Aldrich, Shanghai, China). The efficacy of targeting PHLDB2 in cetuximab treatment was elucidated in CRC cell lines and mouse models.

RESULTS: Based on the transcriptional profile of paired primary and metastatic tumor samples, we identified PHLDB2 as a potential regulator in latent liver metastasis. A detailed mechanistic study showed that chemotherapeutic agent–induced oxidative stress promotes methyltransferase-like 14 (METTL14)-mediated N6-methyladenosine modification of PHLDB2 messenger RNA, facilitating its protein expression. Up-regulated PHLDB2 stabilizes epidermal growth factor receptor (EGFR) and promotes its nuclear translocation, which in turn results in EGFR signaling activation and consequent cetuximab resistance. Moreover, Arg1163 (R1163) of PHLDB2 is crucial for interaction with EGFR, and the R1163A mutation abrogates its regulatory function in EGFR signaling.

CONCLUSIONS: PHLDB2 plays a crucial role in cetuximab resistance and is proposed to be a potential target for the treatment of CRC. *(Cell Mol Gastroenterol Hepatol 2022;13:1223–1242; https://doi.org/10.1016/j.jcmgh.2021.12.011)*

Keywords: EGFR; Latent Metastasis; Cetuximab Resistance; PHLDB2; Colorectal Cancer.

Colorectal cancer (CRC) is one of the most common cancers and the leading cause of cancer-related death worldwide.[1] Although the clinical outcome of CRC patients has improved with early screening and multidisciplinary therapy, metastasis is still the direct cause of death in most CRC patients and frequently develops months or years after treatment for locoregional CRC.[2,3] Latent metastasis is a major hurdle in CRC treatment because these latency competent cancer cells are adaptively resistant to chemotherapy and targeted therapy, retain tumor-initiating potential, and can evolve into systemic metastasis rapidly.[2,4] It has been determined that latent metastasis in patients who already have been treated with chemotherapy is associated with lower response rates,[5] but the underlying mechanism has remained elusive.

A minority of disseminated cancer cells may survive months or years under selective pressure of chemotherapeutic drugs, function as latent seeds, and contribute to metastasis.[6,7] This is of even greater importance given recent evidence supporting early metastatic dissemination in CRC.[8] Latent metastatic cells may acquire survival-related traits as a result of genomic alteration and epigenetic regulation,[9,10] which provides the rationale behind the comparable analysis of paired primary and latent tumor samples in a longitudinal setting. Because the driver gene heterogeneity of metastasis is present only in limited cases,[9,11] most metastatic lesions are indeed regulated at the transcriptional and post-transcriptional levels. As the most prevalent and abundant post-transcriptional RNA modification in eukaryotic messenger, N6-methyladenosine (m^6A) has been shown to play an essential role in human diseases,[12,13] but whether m^6A modification contributes to latent metastasis in CRC is largely unknown.

Cetuximab is a Food and Drug Administration–approved anti–epidermal growth factor receptor (EGFR) monoclonal antibody recommended for metastatic CRC patients with wild-type *KRAS/NRAS/BRAF* tumors,[14,15] but its efficacy remains unsatisfactory, especially in patients with latent metastasis who experience progression on adjuvant therapies, which cannot be readily explained by genetic mechanisms.[14,16] To date, dysregulation of EGFR endocytic trafficking has been linked to the pathogenesis of cancers, but our understanding remains incomplete.[17–20] Thus, it is of paramount importance to elucidate the underlying mechanism of cetuximab resistance in the latent metastasis of CRC.

To unearth the molecular mechanism of latent metastasis, we performed RNA sequencing and transcriptional profiling in tissues from CRC patients and found that the expression of pleckstrin homology-like domain, family B, member 2 (PHLDB2) is up-regulated significantly in latent metastasis of CRC tissues and highly correlated with poor prognosis. Mechanistically, chemotherapeutic drugs, including 5-fluorouracil (5-FU) and oxaliplatin (OXA), induce the expression of PHLDB2 by promoting m^6A modification of PHLDB2 messenger RNA (mRNA). Further analysis showed that PHLDB2 binds and stabilizes EGFR through the Arg1163 site, facilitating EGFR nuclear translocation, thus conferring cetuximab resistance with therapeutic implications.

Results

Identification of PHLDB2 as a Novel Regulator of CRC Progression

To explore the molecular basis for the aggressive behavior of latent metastasis in CRC, latent liver metastasis (LL) that occurred at least 6 months after primary surgery in conjunction with treatment-naïve primary tumors (P) was collected from 5 patients who received postoperative adjuvant treatment, such as capecitabine plus oxaliplatin or 5-fluorouracil, leucovorin, oxaliplatin, while synchronous liver metastasis (SL) with paired primary tumors from 5 CRC patients who underwent simultaneous resection directly with no neoadjuvant treatment received also was obtained as a reference (Figure 1*A*, Supplementary Table 1). To identify potential regulators associated with latent CRC progression, we performed a transcriptomic analysis of paired primary and metastatic tumor tissues from CRC patients. Comparative genome-wide expression analysis yielded a list of genes that were differentially expressed among synchronous or latent liver metastases and their matched primary tumors (ie, SL vs P, SL/P; LL vs P, LL/P; and LL vs SL, LL/SL) using an interaction term between patient group (synchronous or latent) and sample type (primary tumor or liver metastasis) (Figure 1*B*). Based on pathway enrichment analysis, we found concurrent pathways such as cholesterol metabolism enriched in liver metastasis, possibly owing to metabolic reprogramming in liver colonization (Figure 1*C*), which is consistent with previous studies.[21] On the other hand, latent liver metastasis was characterized by enriched signaling pathways, including the phosphatidylinositol 3-kinase protein kinase B (PI3K-AKT) signaling pathway and EGFR tyrosine kinase inhibitor resistance, supporting the rapid progressive course of latent metastasis in response to adjuvant treatment, including EGFR-targeted therapy (Figure 1*A*).

Among the genes that were differentially expressed in both LL/SL and LL/P, *PHLDB2* was the most significant gene (log fold change, >2; adjusted $P < 1 \times 10^{-7}$) (Figure 1*D*,

***Authors share co-first authorship.**

Abbreviations used in this paper: **5-FU, 5-fluorouracil; c-Cbl, Casitas B lymphoma; cDNA, complementary DNA; co-IP, co-immunoprecipitation; CRC, colorectal cancer; EGFR, epidermal growth factor receptor; GFP, green fluorescent protein; IHC, immunohistochemical; LC-MS/MS, liquid chromatography and high-throughput mass spectrometry; LL, latent liver metastasis; METTL, methyltransferase-like; mRNA, messenger RNA; m^6A, N6-methyladenosine; MTT, 3-(4,5-dimethyl-2-thiazolyl)-2,5-diphenyl-2H-tetrazolium bromide; OXA, oxaliplatin; P, primary tumor; PBS, phosphate-buffered saline; PH, pleckstrin homology domain; PHLDB2, pleckstrin homology-like domain, family B, member 2; qRT-PCR, quantitative reverse-transcription polymerase chain reaction; ROS, reactive oxygen species; siRNA, small interfering RNA; TCGA, The Cancer Genome Atlas; WT, wild-type.**

Most current article

2352-345X
https://doi.org/10.1016/j.jcmgh.2021.12.011

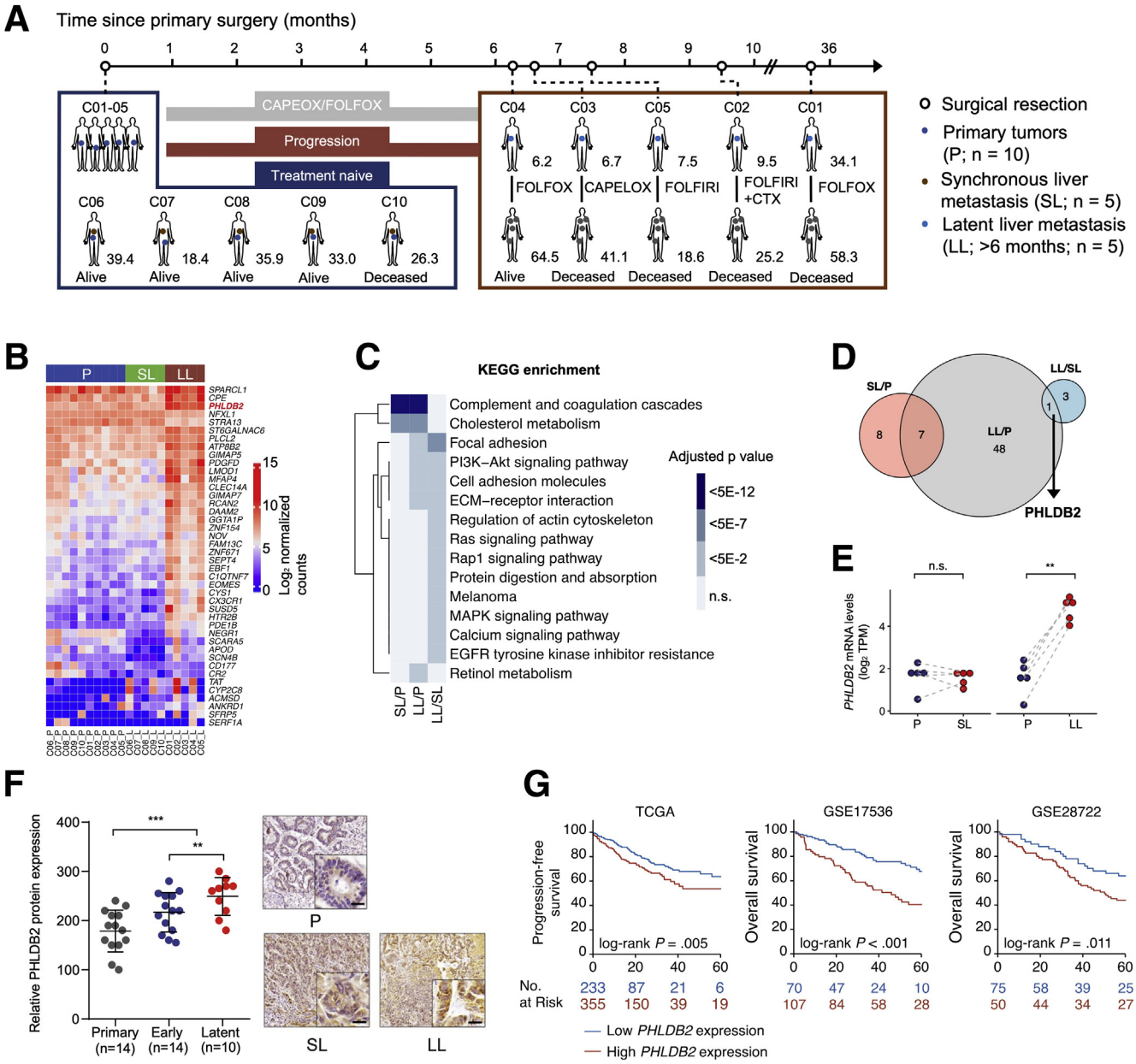

Figure 1. Identification of PHLDB2 as a novel regulator of CRC progression. (*A*) Clinical course. Latent liver metastasis (LL) that occurred after primary surgery in conjunction with treatment-naïve primary tumors (P) were collected from 5 patients who received postoperative adjuvant treatment, such as CAPEOX or FOLFOX, while synchronous liver metastasis (SL) with paired primary tumors from 5 CRC patients who underwent simultaneous resection directly with no neoadjuvant treatment also were obtained as a reference. Numbers on the timeline indicate months relative to the primary surgery. (*B*) Heatmap representation of a list of genes differentially expressed among P, SL, and LL (adjusted $P < .005$, significance was determined using DESeq2 analysis using an interaction term). (*C*) KEGG analysis representing signaling pathways enriched in SL vs P (LL/P), LL vs P (SL/P), and LL vs SL (LL/SL). (*D*) Identification of PHLDB2 as the most significant gene that was increased significantly in latent liver metastasis compared with primary tumor and synchronous liver metastasis (log fold change, >2; adjusted $P < 1 \times 10^{-7}$). (*E*) Relative mRNA levels of PHLDB2 in paired P, SL, and LL ($\log_2$ [TPM + 1]). (*F*) *Left*: The relative protein level of PHLDB2 in P, SL, and LL. *Right*: Representative image of immunohistochemical staining of PHLDB2 in P, SL, and LL. *Scale bars*: 50 μm. (*G*) Kaplan–Meier curves representing the proportion of progression-free or overall survival stratified according to PHLDB2 mRNA levels in CRC patients from 3 independent cohorts (TCGA, GSE17536, and GSE28722). Survival analysis was performed using the log-rank test in panel *G*. $^{**}P < .01$, $^{***}P < .001$. Akt, protein kinase B; CAPEOX, capecitabine plus oxaliplatin; CTX, cetuximab; ECM, extracellular matrix; FOLFIRI, folinic acid, 5-fluorouracil and irinotecan; FOLFOX, 5-fluorouracil, leucovorin, oxaliplatin; MAPK, mitogen-activated protein kinase; PI3K, phosphatidylinositol 3-kinase; Ras, Ras GTPase; Rap1, Rap1 GTPase; TPM, transcripts per million.

Supplementary Table 2), whose mRNA expression was increased significantly in latent liver metastasis compared with primary tumor and synchronous liver metastasis (Figure 1*E*). Consistently, the protein levels of PHLDB2 also were up-regulated in latent liver metastasis, as evidenced by immunohistochemical (IHC) staining (Figure 1*F*). To further address the association between PHLDB2 and CRC progression, we assessed the prognosis of CRC patients in relation to the mRNA level of *PHLDB2* in 3 independent cohorts (ie, The Cancer Genome Atlas, GSE17536, and GSE28722). The results indicated that high expression of *PHLDB2* confers poor overall and progression-free survival (Figure 1*G*). Taken together, these results suggest a potential role of PHLDB2 in latent CRC progression.

Oxidative Stress-Induced m^{6}A Modification Promotes the Expression of PHLDB2

To investigate the mechanism underlying the up-regulation of PHLDB2 in the latent metastasis of CRC patients, we examined both the protein and mRNA levels of PHLDB2 after administration of 5-FU or OXA in 3 CRC cell lines (ie, SW480, DLD-1, and NCI-H508). Consistently higher levels of PHLDB2 were observed after treatment with 5-FU or OXA (Figure 2*A* and *B*). Because the generation of reactive oxygen species (ROS) is a common effect of 5-FU and OXA (Figure 2*C*),[22] we determined whether the ROS scavenger N-acetyl-L-cysteine may reverse this phenomenon. To this end, we found that N-acetyl-L-cysteine attenuated 5-FU–induced or OXA-induced PHLDB2 expression (Figure 2*A* and *B*). Furthermore, Western blot analysis showed that when treated with hydrogen peroxide (H_2O_2) to mimic oxidative stress, PHLDB2 was increased in a time-dependent manner (Figure 2*D*), which also was confirmed by quantitative reverse-transcription polymerase chain reaction (qRT-PCR) (Figure 2*E* and *F*). These results support that overproduction of ROS is responsible for the chemotherapeutic drug 5-FU– or OXA-induced PHLDB2.

Next, we explored the mechanism by which ROS regulate the expression of PHLDB2. In the presence of the transcription inhibitor actinomycin D, the PHLDB2 mRNA degradation rate was evaluated using qRT-PCR for the indicated times. We found that H_2O_2 reduced the degradation of PHLDB2 mRNA (Figure 2*G*), which suggests that treatment with H_2O_2 may facilitate the expression of PHLDB2 by improving its mRNA stability. Because m^{6}A modification is one of the most prevalent modifications in eukaryotic mRNAs and is highly associated with mRNA stability, we investigated the level of m^{6}A modification in PHLDB2 mRNA and found that it was increased significantly in CRC cells treated with H_2O_2 (Figure 2*H*). To determine the underlying mechanism, we analyzed the correlation between *PHLDB2* and m^{6}A writers in CRC using TCGA data. Notably, we found that the m^{6}A writer methyltransferase-like 14 (METTL14) was associated significantly with *PHLDB2* mRNA levels ($R = 0.34$; $P < .001$, Pearson correlation analyses) (Figure 2*I* and *J*), which was validated further by Western blot assays (Figure 2*K*). To confirm whether METTL14 is required for H_2O_2-induced high expression of PHLDB2, we knocked down METTL14 in NCI-H508 cells and found that loss of METTL14 repressed H_2O_2-induced expression of PHLDB2 at both the protein and mRNA levels (Figure 2*L* and *M*). Collectively, these data suggested that up-regulated PHLDB2 in latent metastatic tumor samples may be attributed to METTL14-mediated m^{6}A modification of PHLDB2 mRNA in response to chemotherapeutic treatment.

PHLDB2 Enhances Cetuximab Resistance and Metastatic Potential In Vitro and In Vivo

To ascertain the function of PHLDB2, we constructed DLD-1 and NCI-H508 cells stably overexpressing PHLDB2, and SW480 cells stably knocked down PHLDB2. We found that knockdown of PHLDB2 significantly reduced the levels of EGFR and the phosphorylation levels of EGFR downstream signaling molecules. In contrast, ectopic expression of PHLDB2 led to the activation of EGFR signaling (Figure 3*A*). The 3-(4,5-dimethyl-2-thiazolyl)-2,5-diphenyl-2H-tetrazolium bromide (MTT) assay and colony formation assay were performed, showing that PHLDB2 had no significant effect on CRC cell proliferation (Figure 3*B* and *C*). We next evaluated the effects of PHLDB2 on the metastatic potential of CRC cells and found that migration and invasion were enhanced in PHLDB2-overexpressing cells (Figure 3*D*). In contrast, knockdown of PHLDB2 showed opposite effects (Figure 3*E*). The regulation of metastasis by PHLDB2 in vivo was determined further: DLD-1-Vector or -PHLDB2 cells were injected into the spleen of BALB/c nude mice, and liver metastatic lesions were analyzed by H&E staining. Consistent with the in vitro results, overexpression of PHLDB2 promoted the metastatic capacity of CRC cells (Figure 3*F*).

Given the aggressive nature of latent metastasis in response to adjuvant therapy, including EGFR-targeted therapy, we next analyzed the mRNA expression of *PHLDB2* in 19 CRC cells using the Cancer Cell Line Encyclopedia database in combination with their cetuximab sensitivity based on published reports.[23] As shown in Figure 4*A*, a negative correlation was observed between *PHLDB2* expression and cetuximab efficacy ($r = -0.52$; $P = .023$, Pearson correlation). As such, we hypothesized that PHLDB2 may contribute to cetuximab resistance in CRC cells. To confirm the impact of PHLDB2 on cetuximab efficacy, MTT assays, colony formation assays, and soft agar colony formation assays were performed, showing that PHLDB2 knockdown sensitized SW480 cells to cetuximab, whereas the exogenous expression of PHLDB2 led to a reduction in the cetuximab response rate in DLD-1 and NCI-H508 cells (Figure 4*B*–*E*).

To determine whether PHLDB2 promotes cetuximab resistance by regulating EGFR signaling, the activation of EGFR signaling was evaluated in PHLDB2 overexpression or knockdown cells with or without cetuximab treatment. In the absence of cetuximab, overexpression of PHLDB2 significantly up-regulated the expression of EGFR and the phosphorylation of EGFR downstream molecules, including Akt and extracellular signal–regulated kinase, suggesting activation of EGFR signaling (Figure 4*F* and *G*). In the presence of cetuximab, EGFR signaling was inhibited in PHLDB2-low cells (NCI-H508-vector and SW480-shPHLDB2), but remained unchanged in PHLDB2-high

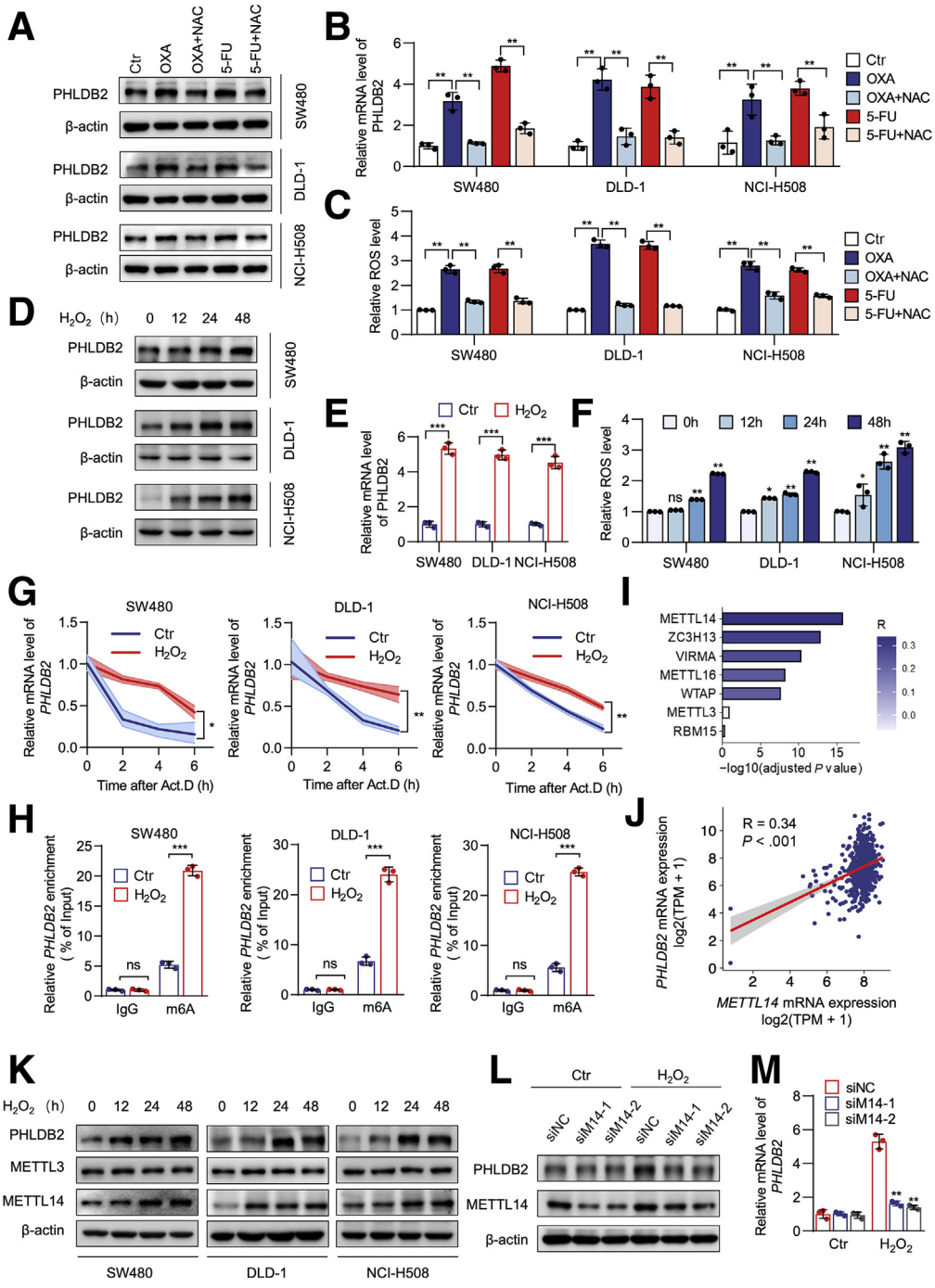

Figure 2. Oxidative stress-induced m^{6}A modification promotes the expression of PHLDB2. (*A*) Protein expression of PHLDB2 was measured by immunoblotting after treatment with 5-FU (2.5 μmol/L) or OXA (5 μmol/L) with or without N-acetyl cysteine (NAC, 2.5 mmol/L) for 24 hours. (*B*) qRT-PCR assays showing the mRNA level of PHLDB2 in the treatment same as Figure 2*A*. (*C*) The level of ROS in CRC cells was measured by flow cytometry after treatment with 5-FU (2.5 μmol/L) or OXA (5 μmol/L) with or without NAC (2.5 mmol/L) for 24 hours. (*D*) The protein level of PHLDB2 was determined by Western blot after treatment with 0.1 mmol/L H_2O_2 for the indicated times. (*E*) The mRNA level of PHLDB2 was determined by qRT-PCR after treatment with 0.1 mmol/L H_2O_2 for 24 hours. (*F*) The level of ROS in CRC cells was measured by flow cytometry after the treatment of 0.1 mmol/L H_2O_2 for the indicated time. (*G*) qRT-PCR assays showing the mRNA degradation rate of PHLDB2 after treatment with actinomycin D (Act D, 2 μg/mL) with or without 0.1 mmol/L H_2O_2 for the indicated time. (*H*) Methylated RNA immunoprecipitation-qPCR (MeRIP-qPCR) analysis was performed to show H_2O_2-mediated PHLDB2 m^{6}A modifications. (*I*) The correlation between *PHLDB2* and mRNA expression of m^{6}A writers was analyzed in CRC using TCGA data. (*J*) The correlation between *PHLDB2* and *METTL14* mRNA expression was analyzed in CRC using TCGA data (r = 0.34; $P < .001$, Pearson correlation). (*K*) Protein levels of METTL3 and METTL14 were determined by immunoblotting after treatment with 0.1 mmol/L H_2O_2 for the indicated times. (*L* and *M*) The protein and mRNA levels of PHLDB2 were detected by Western blot or qRT-PCR with or without H_2O_2 treatment (0.1 mmol/L, 24 hours) in CRC cells transfected with siRNA targeting *METTL14*. *$P <$ .05, **$P <$ .01, ***$P <$ .001. Ctr, Control; siNC, small interfering negative control; TPM, transcripts per million.

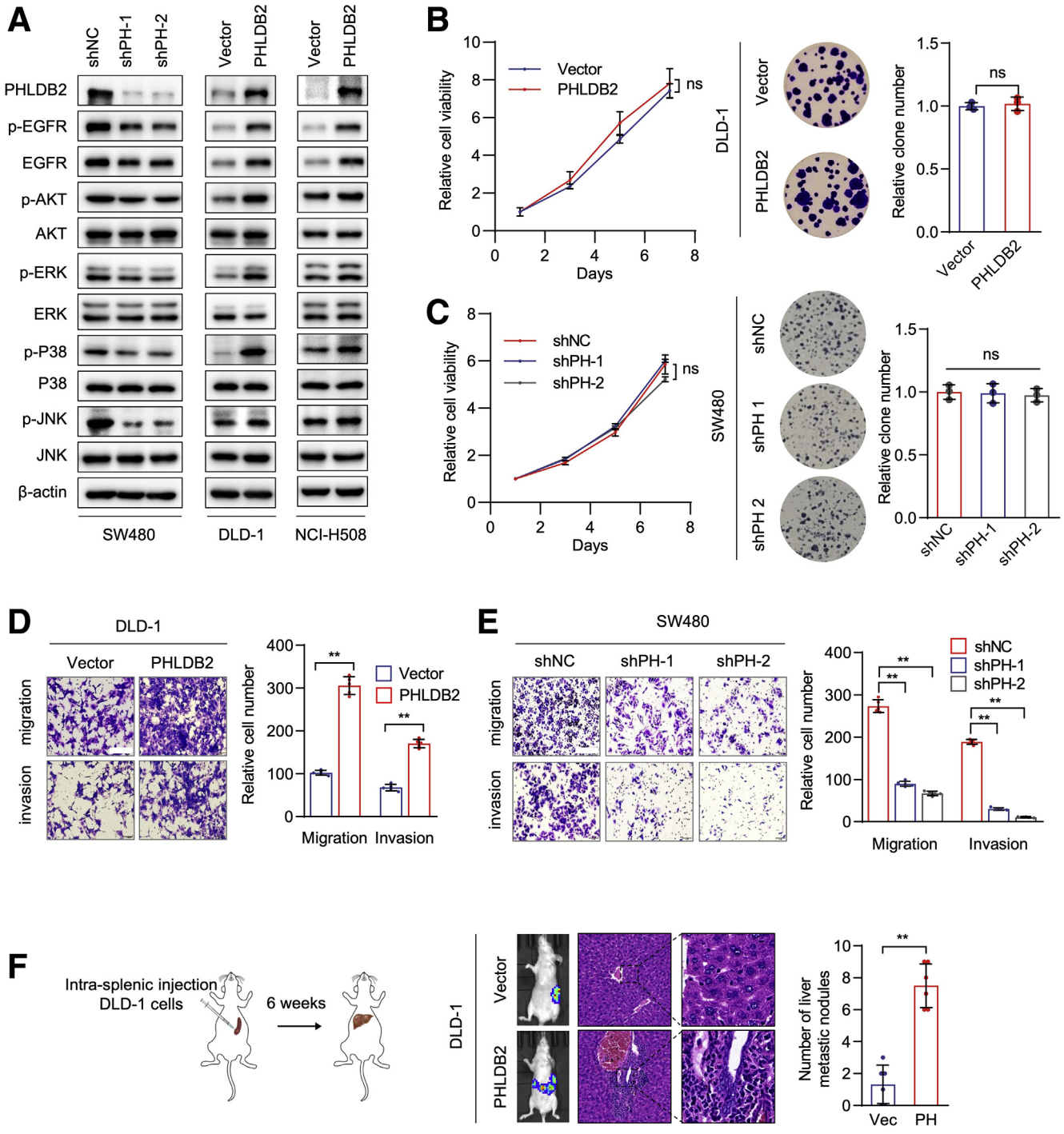

Figure 3. PHLDB2 enhances the metastatic potential of CRC cells. (*A*) PHLDB2-overexpressing and PHLDB2-knockdown stable cells were constructed. (*B* and *C*) Viability of CRC cells were measured by MTT assays at the indicated time and colony formation assays were performed at the indicated time point. (*D* and *E*) Transwell migration and invasion assays were performed with cells transfected with (*D*) PHLDB2 overexpression plasmid, or (*E*) PHLDB2 knockdown plasmid. *Scale bars*: 100 μm. (*F*) Mouse intraspleen injection models of CRC liver metastasis (*left*), and intrasplenic injections assays showing the effects of PHLDB2 on CRC liver metastasis (*right*). *P* values were calculated with the Student *t* test. $^{*}P < .05$, $^{**}P < .01$. ERK, extracellular signal–regulated kinase; p-AKT, phosphorylated protein kinase B; p-EGFR, phosphorylated epidermal growth factor receptor; PH, PHLDB2; shNC, noncoding shRNAs; shPH, shPHLDB2; Vec, Vector.

cells (NCI-H508-PH and SW480-shNC) (Figure 4*F* and *G*). These results indicate that PHLDB2 is sufficient to activate EGFR signaling, and this function overcomes the inhibitory effect of cetuximab on EGFR, thus conferring cetuximab resistance and enhancing metastatic potential in CRC cells. Meanwhile, we evaluated the in vivo impact of PHLDB2 on cetuximab resistance of CRC in BALB/c nude mice in which NCI-H508-Vector or -PHLDB2 cells were injected

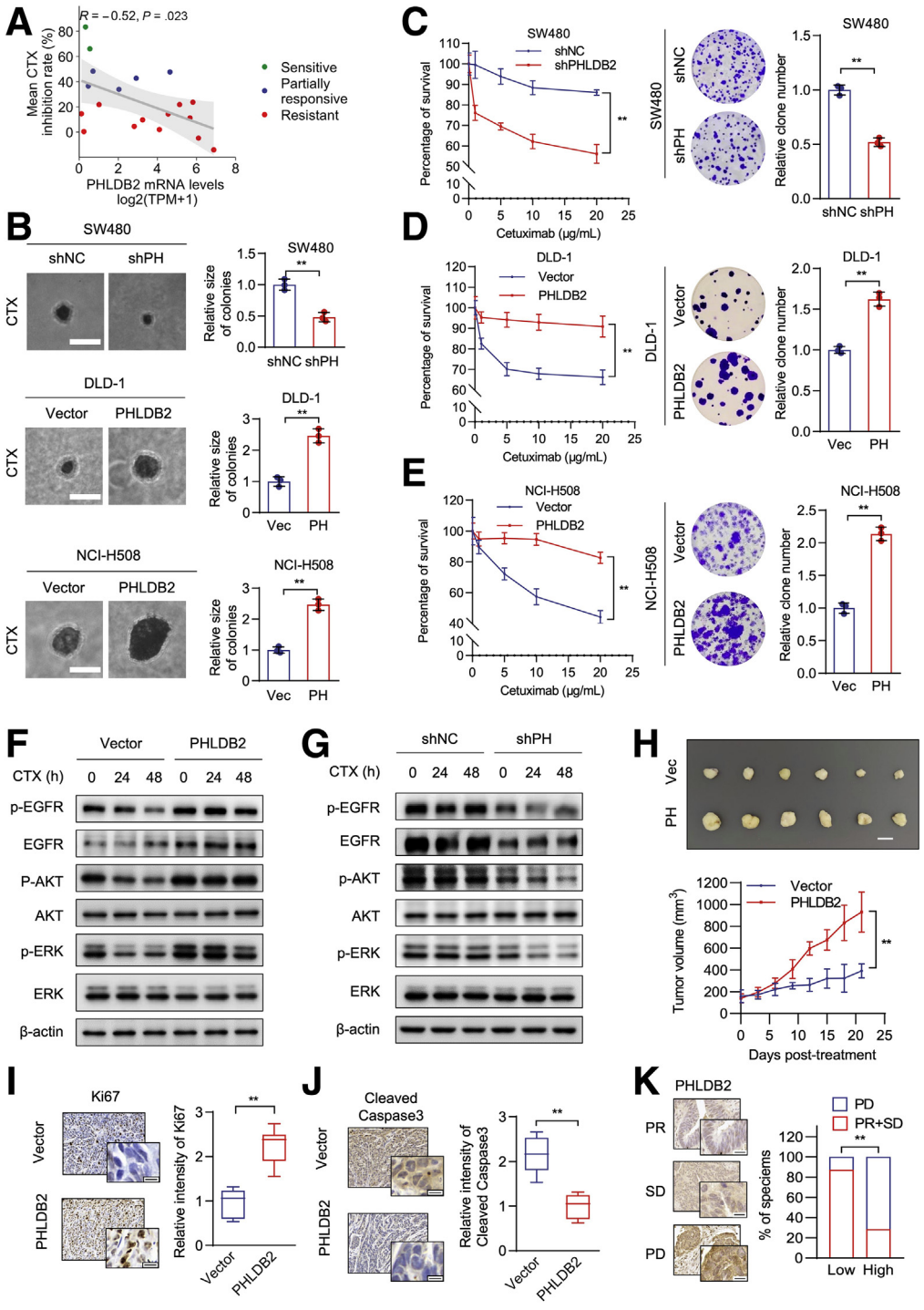

Figure 4. PHLDB2 promotes cetuximab resistance in vitro and in vivo. (*A*) The correlation between the *PHLDB2* mRNA level and cetuximab inhibition rate was analyzed in CRC cell lines using Cancer Cell Line Encyclopedia data. (*B*) The inhibition effect of cetuximab (25 μg/mL) was detected by soft agar colony formation assays (3 weeks). *Scale bars*: 100 μm. (*C–E*) The inhibition rate of cetuximab was detected by MTT (48 hours) or colony formation assays (1 wk). (*F* and *G*) Western blot analysis showing the effects of PHLDB2 on EGFR downstream signaling in (*F*) NCI-H508 and (*G*) SW480 cells treated with cetuximab (25 μg/mL) for the indicated times. (*H*) A subcutaneous xenograft model was established in BALB/c nude mice injected with NCI-H508 vector and NCI-H508 PHLDB2 cells. One week after injection, the diameters of tumors were measured every 3 days. Twenty-one days later, the mice were killed, and the tumors were dissected and photographed. (*I* and *J*) Tumor xenografts in panel *H* were evaluated for the proliferation markers Ki67 and cleaved caspase 3 by immunohistochemistry. *Scale bars*: 50 μm. (*K*) Representative immunohistochemical images showing the PHLDB2 protein levels in human CRC cases treated with cetuximab. $^{*}P < .05$, $^{**}P < .01$, $^{***}P < .001$. *P* values were calculated as follows: (*A*) Pearson correlation, (*B–E*, and *H–J*) Student *t* test, or (*K*) chi-square test, and data are presented as the means ± SD from at least 3 independent experiments. CTX,

subcutaneously in the right flank region. Upon treatment with cetuximab, the anticancer efficacy was decreased significantly in the PHLDB2-overexpression group compared with the vector group (Figure 4*H*). Moreover, overexpression of PHLDB2 led to increased cell proliferation and decreased apoptosis in the presence of cetuximab, as evidenced by IHC staining analysis (Figure 4*I* and *J*). To further explore the correlation between PHLDB2 and cetuximab response, we collected tumor samples from 15 CRC patients administered cetuximab, including 6 progressive disease cases, 6 stable disease cases, and 3 partial response cases. Consistently, patients with higher PHLDB2 expression were enriched significantly in the progressive disease group (Figure 4*K*). Taken together, these results underscore a potential causal role of PHLDB2 in promoting cetuximab resistance and metastasis of CRC cells.

PHLDB2 Protects EGFR From Ubiquitin-Mediated Degradation and Mediates EGFR Nuclear Localization

To understand how PHLDB2 regulates EGFR expression, the protein synthesis inhibitor cycloheximide and proteasome inhibitor MG132 were used to inhibit protein synthesis or block proteasome-mediated protein degradation, respectively. In PHLDB2 knockdown cells, EGFR underwent rapid degradation upon cycloheximide treatment (Figure 5*A*), whereas overexpression of PHLDB2 was shown to stabilize EGFR protein (Figure 5*B*). Consistently, administration of MG132 restored the protein level of EGFR in PHLDB2-low cells (Figure 5*C* and *D*), suggesting that PHLDB2 protects EGFR from proteasome-mediated degradation. In addition, PHLDB2 resulted in a significant decrease in ubiquitin (Figure 5*E*) and the E3 ligase Casitas B-lineage lymphoma (c-Cbl) (Figure 5*F*) conjugated to EGFR, suggesting that PHLDB2 competitively binds with EGFR, dissociates it from its E3 ligase c-Cbl, and thus protects it from degradation. Overall, these data showed that PHLDB2 interacts with EGFR and protects it from ubiquitin-mediated degradation.

Given that cetuximab targets EGFR only in the cell membrane, we postulated that PHLDB2 induces cetuximab resistance by promoting EGFR internalization. Therefore, we determined the localization of EGFR in cells with or without overexpression of PHLDB2. Immunofluorescence assays showed significant enrichment of EGFR in the nucleus in PHLDB2-overexpressing cells (Figure 5*G* and *H*). Moreover, the nuclear localization of EGFR was validated further by a nuclear–cytoplasmic fractionation assay (Figure 5*I* and *J*). To explore the molecular mechanism by which PHLDB2 promotes the nuclear translocation of EGFR, we detected the expression of Rab11A, a well-known EGFR recycling protein involved in EGFR recycling back to the plasma membrane,[24] and found that PHLDB2 reduced the binding affinity between Rab11A and EGFR (Figure 5*K*). In addition, overexpression of PHLDB2 enhanced the activation of Src kinase (Src) (Figure 5*L*), which has been reported to mediate the nuclear translocation of EGFR.[25] To further confirm the phenotype by which PHLDB2 promotes EGFR nuclear translocation, we determined the expression of the nuclear EGFR downstream target genes Myb-related protein B (B-myb), Aurora A kinase (AURKA), Aurora B kinase (AURKB), and cyclin D1. As shown in Figure 5*M*, qRT-PCR analysis showed that PHLDB2 promotes nuclear EGFR-mediated transcription, as evidenced by the increased mRNA levels of nuclear EGFR downstream target genes. Overall, these data confirmed that PHLDB2 facilitates EGFR nuclear localization, which might contribute to cetuximab resistance.

Arg1163 Is Required for the Interaction of PHLDB2 With EGFR

To elucidate the mechanism underlying PHLDB2-mediated EGFR nuclear localization, PHLDB2 interactors were coimmunoprecipitated (Figure 6*A*) and subjected to rounds of liquid chromatography and high-throughput mass spectrometry (LC-MS/MS). Then, the identified binding partners overlapped with the structure-based protein–protein interaction database,[26] suggesting EGFR as the top hit among the 4 potential PHLDB2 interactors (Figure 6*B*, Supplementary Tables 3 and 4). The interaction of PHLDB2 with EGFR was confirmed further by co-immunoprecipitation (co-IP) (Figure 6*C* and *D*) and proximity ligation assays (Figure 6*E*). To investigate the molecular basis for the interaction between PHLDB2 and EGFR, we first produced a series of Flag-tagged PHLDB2 truncated mutants according to the literature[27] (Figure 6*F*). In HEK293T cells, each truncated mutant reached a similar and reproducible intensity of protein. Co-immunoprecipitated green fluorescent protein (GFP)-tagged EGFR was observed only in fragments containing the Pleckstrin homology domain (ie, full-length, △1-305, △306-562, and △563-916), indicating that the PH domain of PHLDB2 is required for binding to EGFR (Figure 6*G*). To further identify the binding site mediating the interaction, molecular docking with ZDOCK calculations was conducted to make a prediction. As a result, we found that the Arg1163 site of PHLDB2, which is localized in the PH domain, may be responsible for its binding to EGFR (Figure 6*H*). This prediction was validated further by co-IP assays in cells transfected with wild-type (WT) or R1163A mutant PHLDB2, in which the R1163A mutation significantly abolished the binding of PHLDB2 to EGFR (Figure 6*I*). Moreover, the R1163A-mediated binding behavior in CRC cells also was confirmed by Duolink (Sigma-Aldrich, Shanghai, China) in situ proximity ligation assays (Figure 6*J*).

In addition, we also investigated the binding sites of EGFR based on molecular docking modeling, which

cetuximab; ERK, extracellular signal–regulated kinase; P-AKT, phosphorylated protein kinase B; p-EGFR, phosphorylated epidermal growth factor receptor; p-ERK, phosphorylated extracellular-regulated kinase; PD, progressive disease; PH, PHLDB2; PR, partial response; SD, stable disease; shNC, noncoding shRNAs; shPH, shPHLDB2; TPM, transcripts per million; Vec, Vector.

suggested that the H988 and S991 residues of EGFR mediate the interaction with PHLDB2 (Figure 6*H*). To confirm this, Flag-tagged WT, H988A mutated, S991A mutated, and H988A/S991A double-mutated EGFR were tested for the interaction with PHLDB2. Co-IP assays showed that S991A and H988A/S991A double-mutated EGFR significantly abolished the binding of EGFR to PHLDB2 (Figure 6*K*), indicating that S991 of EGFR is required for the interaction with PHLDB2. Together, these data showed that R1163 of PHLDB2 and S991 of EGFR mediate their interaction.

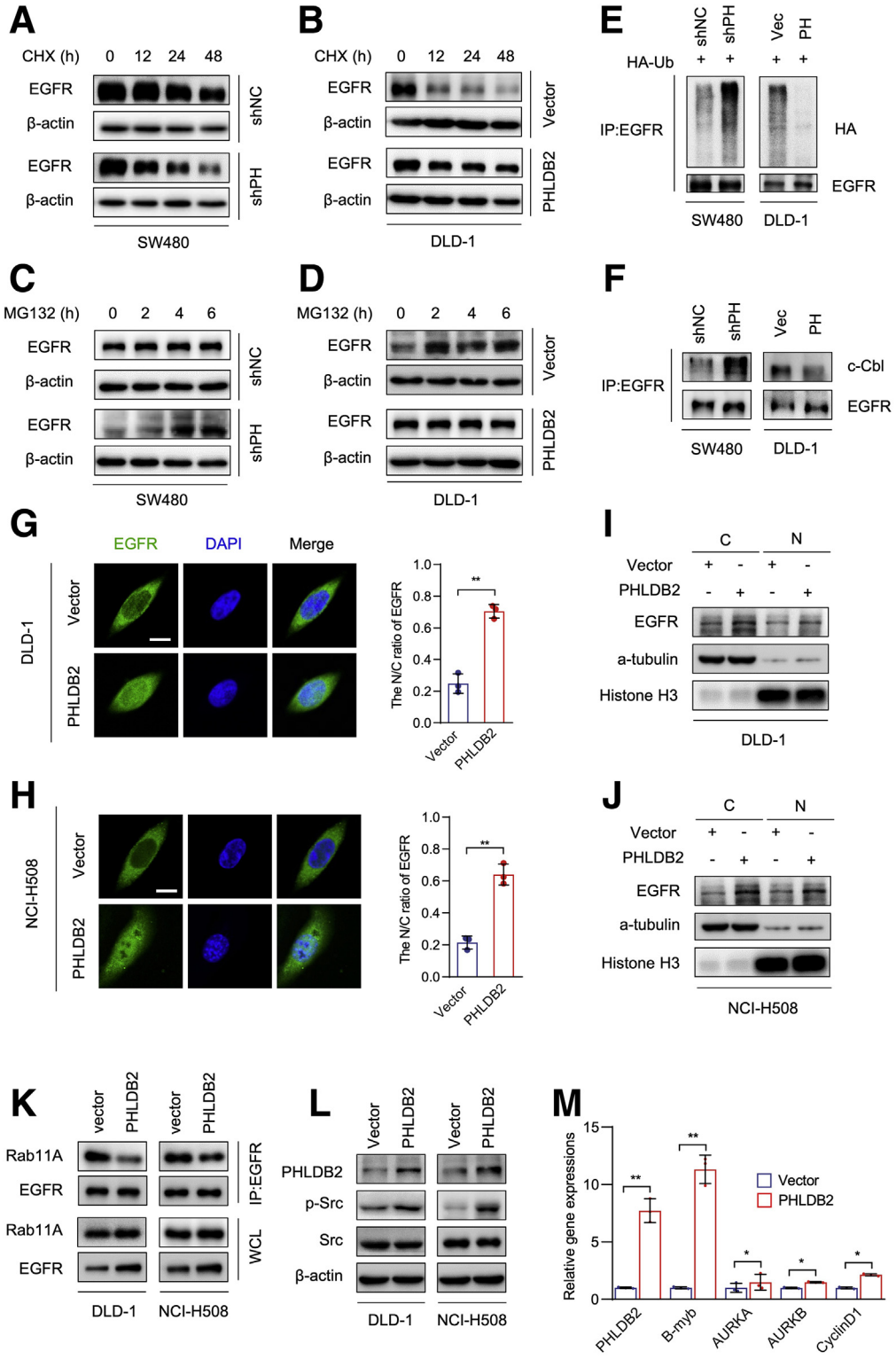

R1163A Mutation Diminishes PHLDB2-Mediated Cetuximab Resistance Both In Vitro and In Vivo

To determine whether the R1163-mediated interaction with EGFR confers the biological function of PHLDB2, we first evaluated the effect of the R1163A mutation on EGFR signaling, and found that R1163A mutation significantly reduced the levels of EGFR and the phosphorylation levels of EGFR downstream signaling molecules compared with ectopic expression of WT PHLDB2 (Figure 7*A*). Notably, the R1163A mutation also attenuated the PHLDB2-enhanced metastatic potential of CRC cells (Figure 7*D* and *E*), but neither WT PHLDB2 nor R1163A-mutant PHLDB2 affected cell proliferation (Figure 7*B* and *C*). On the other hand, R1163A-mutated PHLDB2 failed to activate EGFR signaling regardless of the presence of cetuximab (Figure 8*A* and *B*). In addition, mutation of R1163 abrogated the function of PHLDB2 to promote the nuclear localization of EGFR (Figure 8*C*). Consistently, R1163A-mutated PHLDB2 no longer conferred a phenotype resistant to cetuximab in CRC cells compared with WT PHLDB2 (Figure 8*D*–*G*).

To determine the effects of the PHLDB2 R1163A mutation in vivo, a xenograft mouse model was used to evaluate the cetuximab response rate. Consistent with the in vitro findings, overexpression of WT PHLDB2 conferred cetuximab resistance, whereas the R1163A mutant failed to induce obvious cetuximab resistance compared with the vector group (Figure 8*H*). In addition, overexpression of PHLDB2 with mutated R1163A led to increased apoptosis and decreased cell proliferation in response to cetuximab compared with overexpression of WT PHLDB2, as evidenced by IHC staining analysis (Figure 8*I* and *J*). Taken together, these data supported that Arg1163 of PHLDB2 mediated its function in EGFR signaling and cetuximab resistance both in vitro and in vivo.

Discussion

The clinical observation that metastases may develop after months or years on adjuvant therapy after primary surgery underscores the necessity to evaluate the impact of adjuvant therapy on the development of latent metastasis.[2,4] In the present work, we describe a mechanism involved in latent metastasis of CRC. Based on the transcriptional profiling of paired primary tumors and synchronous or metachronous metastases, we identified PHLDB2 as a potential regulator of latent metastasis that is up-regulated in response to adjuvant treatment. Our further work uncovered a role for PHLDB2 in regulating EGFR signaling pathways, thereby facilitating cetuximab resistance and tumor progression.

PHLDB2 (pleckstrin homology-like domain, family B, member 2), a 160-kilodalton protein that contains a PH domain and 2 coiled-coil domains,[27,28] has been shown to regulate the migration and invasion of cancer cells.[28–30] Here, we show that PHLDB2 is up-regulated significantly in latent metastasis of CRC, and increased PHLDB2 levels are associated with poor survival outcomes, possibly owing to aggressive behavior and treatment resistance. Mechanistically, chemotherapeutic agent–induced ROS promote m^6A modification of PHLDB2 mRNA. As one of the most prevalent and abundant post-transcriptional RNA modifications in mRNA, m^6A modification appears to be an early adaptive mechanism by which cancer cells respond to chemotherapeutic agent–induced oxidative stress.[31–33] Together, our data show that chemotherapeutic agent–induced ROS promote the expression of PHLDB2 via m^6A modification, resulting in latent metastasis.

As a key driver of CRC tumorigenesis, the aberrant activity of EGFR in the initiation and progression of CRC underscores the importance of characterizing its regulatory network. Known as a prototypic receptor tyrosine kinase, EGFR endocytic trafficking also has been implicated in the regulation of EGFR activation, including recycling and degradation. In this study, we identified that PHLDB2 binds to the Ser991 site of EGFR, resulting in a significant decrease in ubiquitin and the E3 ligase c-Cbl conjugated to EGFR, thus suppressing ubiquitin-mediated degradation of EGFR. This is consistent with previous quantitative mass spectrometric analyses showing the association between Ser991 and ubiquitin-mediated degradation of EGFR, in which the S991A mutation decreases conjugated ubiquitin on EGFR.[34] The activation of EGFR and its downstream signaling pathways ultimately may promote CRC cell proliferation and migration, thus making it one of the most important molecular targets in CRC treatment.[35–37]

Cetuximab is a Food and Drug Administration–approved EGFR monoclonal antibody that binds to the extracellular domain of EGFR and promotes receptor internalization and degradation.[35,38] Although cetuximab currently is

Figure 5. PHLDB2 protects EGFR from ubiquitin-mediated degradation and mediates EGFR nuclear localization. (*A*–*D*) Effects of PHLDB2 on EGFR protein stability were detected in PHLDB2 overexpression or knockdown CRC cells. Cells were treated with (*A* and *B*) 10 μg/mL cycloheximide (CHX) or (*C* and *D*) 25 μmol/L MG132 to inhibit protein synthesis or degradation at the indicated time points, respectively. (*E*) Hemagglutinin-ubiquitin (HA-Ub) was transiently transfected into PHLDB2 overexpression or knockdown CRC cells, followed by co-IP assays to determine the ubiquitination of EGFR. Cells were treated with 25 μmol/L MG132 for 4 hours before harvest. (*F*) Co-IP assays showing the interaction between EGFR and its E3 ligase c-Cbl regulated by PHLDB2 expression. (*G* and *H*) Immunofluorescence assays were performed to determine the subcellular localization of EGFR in the indicated stable cells. *Right*: Quantification of the relative nuclear/cytoplasmic ratio of EGFR. *Scale bars*: 50 μm. (*I* and *J*) Cell nucleus/cytoplasm fractions were immunoblotted to determine EGFR localization. a-Tubulin and histone H3 were used as cytoplasmic and nuclear markers, respectively. (*K*) co-IP assays show that the interaction between EGFR and Rab11A was affected by PHLDB2 expression. (*L*) The phosphorylation and expression of Src protein were detected by immunoblotting. (*M*) mRNA levels of nuclear EGFR target genes, including B-myb, AURKA, AURKB, and cyclin D1, were quantitated by qRT-PCR. $^*P < .05$, $^{**}P < .01$. (*G*, *H*, and *M*) *P* value was calculated by the Student *t* test, and data are presented as the means ± SD from at least 3 independent experiments. AURKA, Aurora A kinase; AURKB, Aurora B kinase; B-myb, Myb-related protein B; C, cytoplasm; DAPI, 4′,6-diamidino-2-phenylindole; N, nucleus; N/C, nucleus/cytoplasm; PH, PHLDB2; shNC, noncoding shRNAs; shPH, shPHLDB2; Src, Src kinase; Vec, Vector; WCL, whole cell lysate.

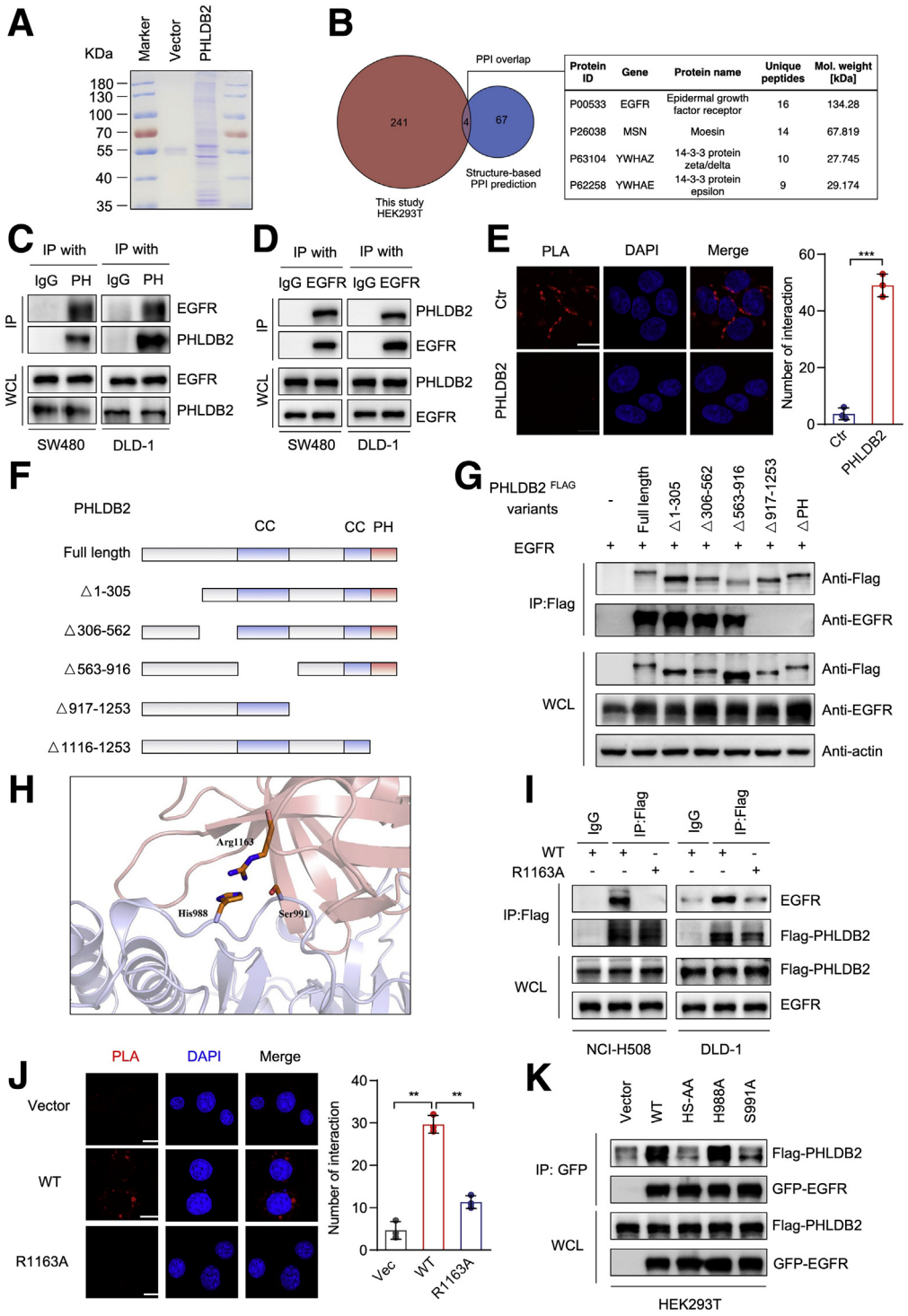

Figure 6. Arg1163 is required for the interaction of PHLDB2 with EGFR. (*A*) Total lysates from HEK293T cells with or without ectopic expression of Flag-tagged PHLDB2 were co-immunoprecipitated with anti-Flag affinity agarose, followed by sodium dodecyl sulfate–polyacrylamide gel electrophoresis and Coomassie brilliant blue staining. (*B*) The overlap between the protein–protein interactome and LC–MS/MS data show the potential interaction partners of PHLDB2. (*C* and *D*) Co-IP assays indicate the interaction between PHLDB2 and EGFR in CRC cells. (*E*) Proximity ligation assay (PLA) showing the interaction between PHLDB2 and EGFR in NCI-H508 cells. *Scale bar*: 10 μm. (*F*) Schematic diagram of PHLDB2 and the truncated PHLDB2 fragments. The numbers represent amino acid residues. (*G*) Co-IP assay showing the interaction between EGFR and PHLDB2 truncations in HEK293T cells. (*H*) Molecular docking of 3-dimensional structures predicts the binding of PHLDB2 (red) with EGFR (gray). (*I* and *J*) The interaction between EGFR and WT or R1163A-mutated PHLDB2 was determined by (*I*) co-IP assays and (*J*) PLA assays. (*K*) Co-IP assays were performed to evaluate the interaction between PHLDB2 and WT or mutated EGFR in HEK293T cells. $^{**}P < .01$, $^{***}P < .001$. (*E*) *P* value was calculated by Student *t* test, and data are presented as the means ± SD from at least 3 independent experiments. CC, coiled-coil domain; Ctr, control; DAPI, 4′,6-diamidino-2-phenylindole; PH, pleckstrin homology-like domain; Vec, vector; WCL, whole cell lysate.

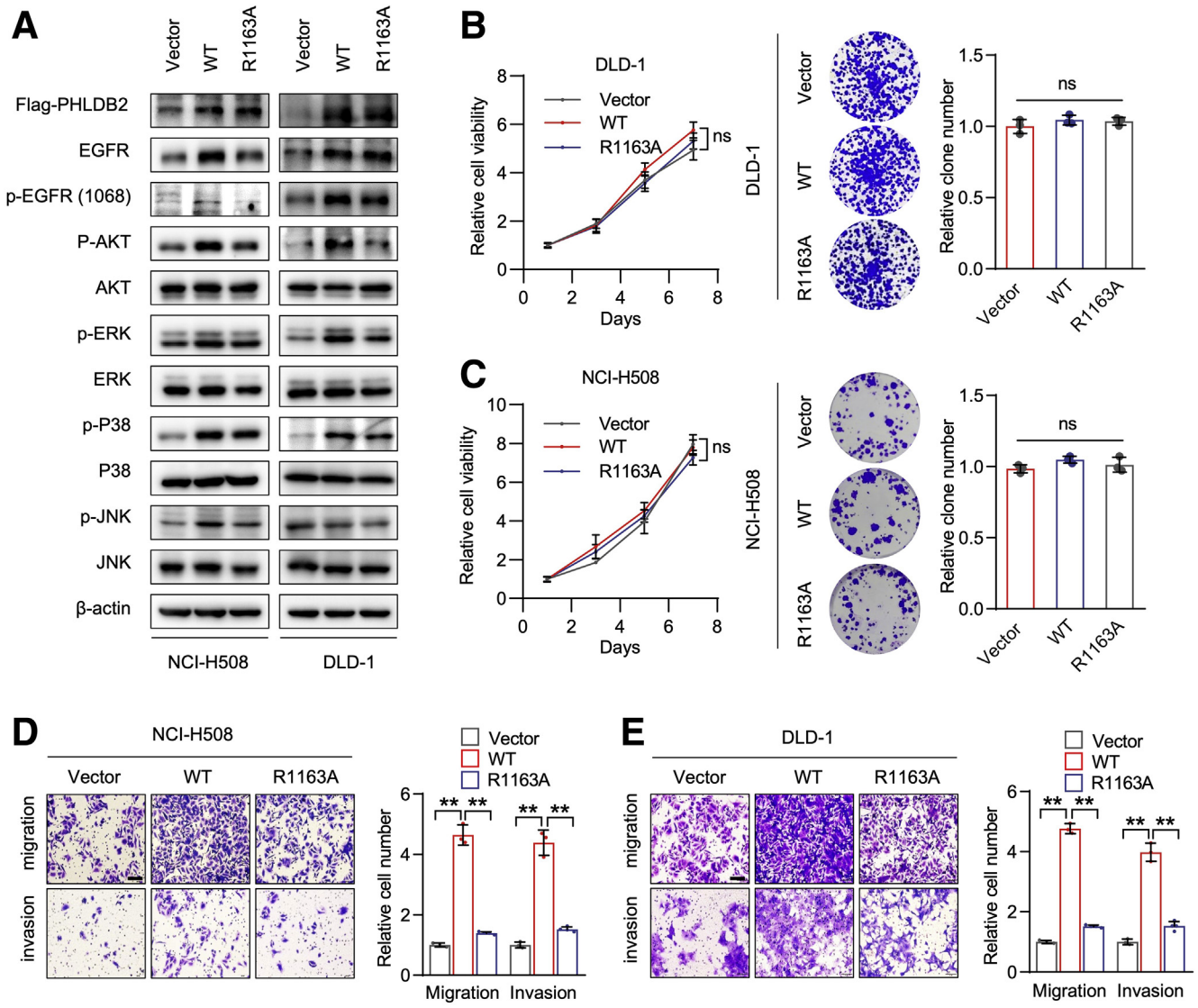

Figure 7. R1163A mutation abrogates PHLDB2-mediated tumor metastasis. (*A*) Immunoblotting assays determined the effects of WT and R1163A (RA)-mutated PHLDB2 on EGFR downstream signaling. (*B* and *C*) MTT assays and colony formation assays were performed to determine cell growth of CRC cells. (*D* and *E*) Transwell migration and invasion assays were performed in cells transfected with vector, PHLDB2 WT, or R1163A. *Scale bars*: 100 μm. Values are means ± SD. *P* values were calculated with the Student *t* test. $^{**}P < .01$. AKT, protein kinase B; ERK, extracellular signal–regulated kinase; JNK, c-Jun N-terminal kinase; P-AKT, phosphorylated protein kinase B; p-ERK, phosphorylated extracellular signal–regulated kinase; p-JNK, phosphorylated c-Jun N-terminal kinase.

recommended for metastatic CRC patients who experience progression on therapies such as 5-fluorouracil, leucovorin, oxaliplatin or capecitabine plus oxaliplatin without EGFR inhibitors, the results of our study justify a negative role of adjuvant therapy with respect to cetuximab efficacy in latent metastasis. As the direct target of cetuximab, EGFR expression has been proposed as a potential marker of clinical efficacy in early trials with cetuximab.[39] However, the correlation between EGFR expression and cetuximab response is not evident in CRC,[14,40,41] and the underlying mechanism that mediates resistance to EGFR-targeted therapy remains largely elusive.

Although EGFR is retained primarily along the plasma membrane, several studies have documented the nuclear localization of EGFR, wherein it functions as a transcription factor and a potential mechanism of resistance to EGFR inhibitor.[42,43] Nuclear translocation of EGFR has been observed in cetuximab-resistant non–small cell lung cancer cells,[42] but its role in CRC remains unclear, thus understanding the mechanism of EGFR nuclear translocation may enable the development of a new therapeutic strategy for CRC. Here, we found that PHLDB2 interacts with and stabilizes EGFR, facilitating its nuclear translocation and leading to cetuximab resistance in CRC cells. It has been determined that the phosphorylation-deficient variant S991A may impair receptor endocytosis, and phosphorylation of EGFR at site Ser991 determines the trafficking of EGFR.[34] Consistently, we found that PHLDB2 reduced the

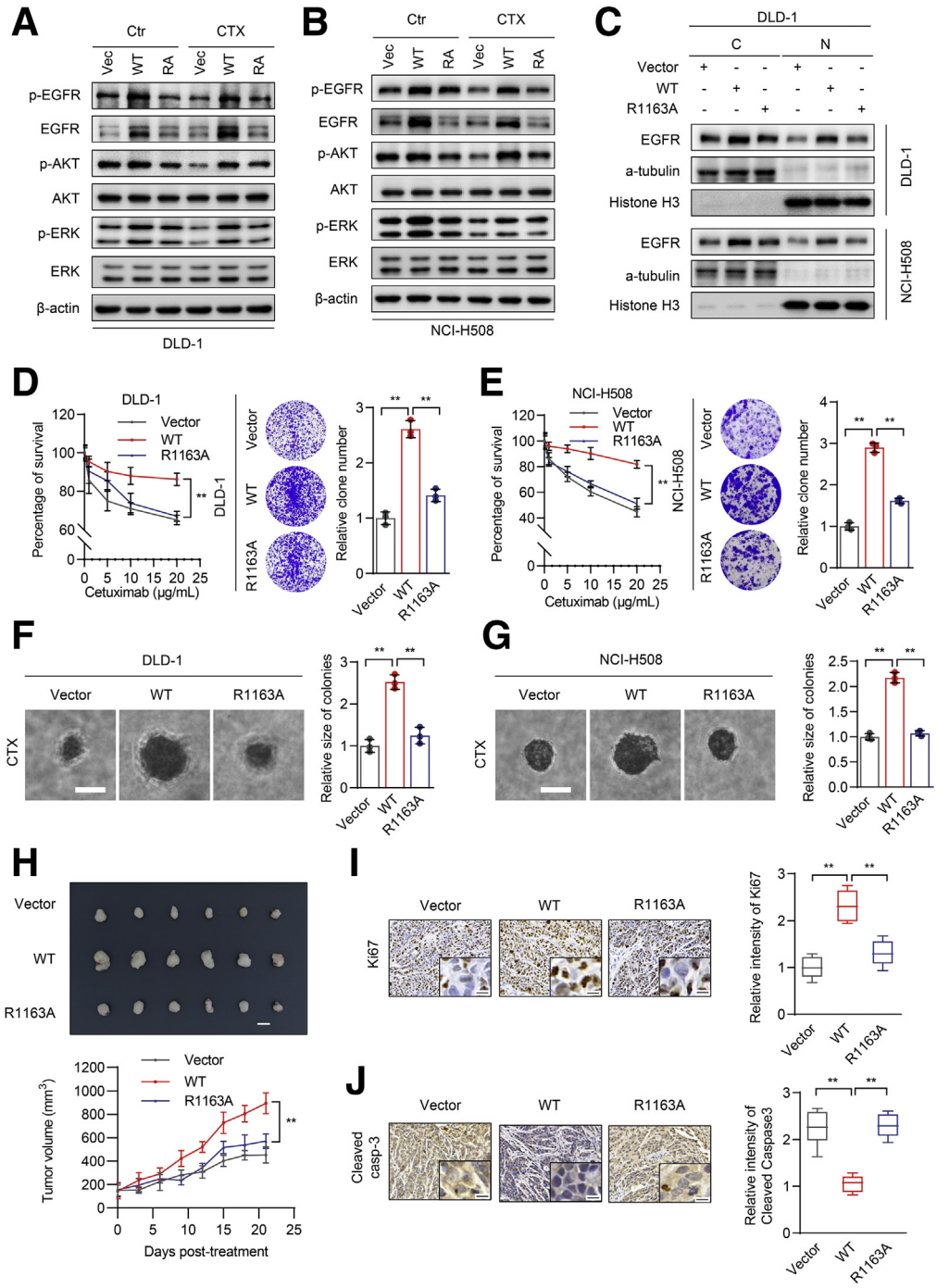

Figure 8. R1163A mutation diminishes PHLDB2-mediated cetuximab resistance both in vitro and in vivo. (*A* and *B*) Immunoblotting showing the phosphorylation and expression of the indicated proteins in WT or R1163A-mutated (RA) cells with or without 20 μg/mL cetuximab (CTX) treatment for 24 hours. (*C*) Cell nucleus/cytoplasm fractions were immunoblotted to determine EGFR localization in WT or R1163A-mutated cells. (*D* and *E*) MTT and colony formation assays were performed to determine the viability of the indicated cells in response to cetuximab treatment. (*F* and *G*) Soft agar colony formation assays were performed to determine the viability of the indicated cells in response to CTX (20 μg/mL) treatment. (*H*) A subcutaneous xenograft model was established in BALB/c nude mice injected with vector, PHLDB2 WT, and PHLDB2 RA NCI-H508 cells. One week after injection, the diameters of the tumors were measured every 3 days. Twenty-one days later, the mice were killed, and the tumors were dissected and photographed. (*I* and *J*) The protein levels of Ki67 and cleaved caspase 3 were detected by immunohistochemistry. *Scale bars*: 50 μm. $^{**}P < .01$. (*D*–*J*) *P* values were calculated by Student *t* test. Data are presented as the means ± SD from at least 3 independent experiments. AKT, protein kinase B; C, cytoplasm; Ctr, control; ERK, extracellular signal–regulated kinase; N, nucleus; p-AKT, phosphorylated protein kinase B; p-ERK, phosphorylated extracellular signal–regulated kinase; Vec, vector.

Table 1. Antibodies and Reagents

Reagent	Source	Identifier
Antibodies		
PHLDB2 (1:200 [IF],1:1000 [WB])	Novus	NBP2-38238
METTL3 (1:1000)	Abcam	ab195352
METTL14 (1:1000)	Abcam	ab220030
β-actin (1:2000)	Santa Cruz Biotechnology	sc-69879
ERK (1:1000)	Cell Signaling Technology	4695
p-ERK (1:1000)	Cell Signaling Technology	4370
JNK (1:1000)	Cell Signaling Technology	9252
AKT (1:1000)	Cell Signaling Technology	9272
p-AKT (1:1000)	Cell Signaling Technology	4060
P38 (1:1000)	Cell Signaling Technology	8690
p-P38 (1:1000)	Cell Signaling Technology	4511
EGFR (1:1000)	Cell Signaling Technology	4267
EGFR (1:100)	Santa Cruz Biotechnology	sc-373746
p-EGFR (1:1000)	Cell Signaling Technology	3777
Ki67	Abcam	ab16667
Cleaved caspase 3	Cell Signaling Technology	9664
HA (1:1000)	Abcam	ab18181
c-Cbl (1:1000)	Cell Signaling Technology	2747
GFP (1:1000)	Cell Signaling Technology	2955
α-tubulin (1:1000)	Cell Signaling Technology	2144
Histone H3 (1:1000)	Cell Signaling Technology	4499
Src (1:1000)	Cell Signaling Technology	2109
p-Src (1:1000)	Cell Signaling Technology	59548
Rab11A (1:1000)	Cell Signaling Technology	5589
Flag (1:1000)	Cell Signaling Technology	14793
Reagents		
Cycloheximide	Beyotime	SC0353
MG132	Beyotime	S1748
Actinomycin D	Sigma-Aldrich	SBR00013
Hydrogen peroxide solution	Sigma	323381
Lipo3000 Transfection Reagent	Thermo Fisher Scientific	L3000015
DAPI	Thermo Fisher Scientific	62248
MTT	Sigma	M2128
DMSO	Sigma	D2650

AKT, protein kinase B; DAPI, 4′,6-diamidino-2-phenylindole; DMSO, dimethyl sulfoxide; ERK, extracellular signal–regulated kinase; HA, hemagglutinin; JNK, c-Jun N-terminal kinases; p-AKT, phosphorylated protein kinase B; p-EGFR, phosphorylated epidermal growth factor receptor; p-ERK, phosphorylated extracellular signal–regulated kinase; p-SRC, phosphorylated Src kinase; SRC, Src kinase; WB, western blot.

binding affinity between EGFR and Rab11A, a well-known EGFR recycling protein involved in EGFR trafficking.[20] Together, our findings provide a molecular basis for PHLDB2-mediated nuclear translocation of EGFR.

In summary, our data suggest a key role of PHLDB2 in mediating latent progression of CRC by modulating EGFR signaling. The up-regulation of PHLDB2 is attributed to METTL14-mediated m^6A modification induced by chemotherapeutic agents. Mechanistically, PHLDB2 interacts with and stabilizes EGFR, facilitating its nuclear translocation and leading to cetuximab resistance. Thus, our findings implicate PHLDB2 as a potential marker and therapeutic target for latent metastatic CRC, providing a rationale for designing inhibitors targeting PHLDB2 as a novel approach for CRC treatment.

Materials and Methods

Antibodies and Reagents

The antibodies and reagents used in this study are listed in Table 1.

Patients

Human CRC tissue samples were obtained from the BioBank of West China Hospital (Chengdu, China). To investigate the molecular characteristics of latent metastases, we selected 5 CRC cases with latent metastasis and collected their treatment-naïve primary tumor and liver metastasis that occurred at least 6 months after primary surgery. Tumor tissues from 5 patients who underwent concurrent resection of the primary tumor and liver metastases without neoadjuvant therapy also were collected as a reference. To validate the expression of PHLDB2, 38 tumor samples from 31 metastatic CRC patients who underwent surgical resection also were obtained for immunohistochemistry (Figure 1*F*). In addition, tumor samples from 15 CRC patients administered cetuximab were included to address the association between PHLDB2 expression and cetuximab response (Figure 3*K*). Written informed consent was obtained from all patients. This study was approved by the Ethics Committee of West China Hospital, Sichuan University (2019 [338]; 2020 [374]).

Cell Lines

SW480, DLD-1, NCI-H508, and HEK293T cells were purchased from the American Type Culture Collection. Short tandem repeat analysis was performed for each of these cell lines. SW480, DLD-1, and HEK 293T cell lines were propagated in Dulbecco's modified Eagle medium (Gibco, Shanghai, China); the NCI-H508 cell line was propagated in RPMI (Gibco, Shanghai, China). All cell lines were maintained in media supplemented with 10% fetal bovine serum (Biological Industries), 100 U/mL penicillin, and 100 μg/mL streptomycin (HyClone, Logan, UT) in a humidified incubator at 37°C under 5% CO_2.

Animal Studies

All animal procedures were approved by the Institutional Animal Care and Treatment Committee of Sichuan University. BALB/c nude female mice (age, 6 wk) were purchased from HFK Bioscience Co, Ltd (Beijing, China). Mice were housed in laminar flow cabinets under specific pathogen-free conditions with free access to water and food, under the room illumination cycle for a 12-hour light-dark cycle. For the subcutaneous CRC xenograft model, suspensions of the corresponding NCl-H508 cells were injected subcutaneously into the flanks (1×10^7 tumor cells/100 μL phosphate-buffered saline [PBS] per spot; 6 mice in each group). When the tumor volume reached approximately 100 mm^3, mice were administered 0.2 mL cetuximab (50 mg/kg in physiological saline, intraperitoneal injection, every 3 days). Animals were weighed, and the tumor size was measured using caliper measurements daily. Tumor volume was calculated using the following formula: volume = $(L \times W^2)/2$, where L = length and W = width. For spleen injection, mice were anesthetized with chloral hydrate and the spleen was exteriorized via a small left-side abdominal incision. DLD-1 cells (-vector or -PHLDB2) were injected slowly into the spleen (1×10^6 tumor cells/50 μL PBS per spot). The muscle incision was closed with continuous absorbable sutures and the skin incision was closed with simple nonabsorbable sutures. To measure the luciferase intensity of injected cells, 2.25 μg/mL luciferin was injected intraperitoneally and luciferase activity was assessed 5 minutes after luciferin injection using an IVIS Spectrum Pre-clinical in vivo Imaging System (IVISSPE; PerkinElmer, Waltham, MA) machine.

Immunoblotting and Immunoprecipitation

Proteins were extracted using RIPA buffer (150 mmol/L NaCl, 50 mmol/L Tris-HCl [pH 7.5], 1 mmol/L EDTA, 0.25% Na-deoxycholate, and 1% NP-40) supplemented with protease inhibitors and phosphatase inhibitors (B14001 and B15001; Beyotime, Shanghai, China), and quantified using the BCA assay (23250; Thermo Fisher Scientific, Waltham, MA). Sodium dodecyl sulfate–polyacrylamide gel electrophoresis was performed to separate proteins, which then were transferred to polyvinylidene difluoride membranes (ISEQ00010; EMD Millipore, Burlington, MA). Next, the membranes were blocked in 5% fat-free milk for 2 hours and incubated with primary antibodies at 4°C overnight. After washing the membranes, secondary antibodies labeled with horseradish peroxidase (Santa Cruz Biotechnology, Dallas, TX) were applied at room temperature for 2 hours and the immunoreactivity was visualized by ECL (WBKLS0500; EMD Millipore, Burlington, MA). For immunoprecipitation, cells were collected and lysed with IP lysis buffer (100 mmol/L NaCl, 20 mmol/L Tris-HCl, 0.5 mmol/L EDTA, pH 7.4, and 0.5% NP-40). After centrifugation, the indicated antibodies (1 μg) were subjected to rotation overnight at 4°C. Then lysates were incubated with protein A Sepharose (17–0963-03; GE Healthcare, Chicago, IL) or protein G agarose (16-266; Millipore) for 3 hours, followed by centrifugation, washed 4 times using binding buffer (150 mmol/L NaCl, 20 mmol/L Tris-HCl, 0.5 mmol/L EDTA, pH 7.4, and 0.5% NP-40), and boiled with loading buffer for immunoblotting analysis.

MTT and Colony Formation Assay

For MTT assay, cells were seeded at 3×10^3 cells/100 μL/well in 96-well plates and treated as indicated. A total of 10 μL MTT (5 mg/mL in PBS) was added to each well and cells were incubated at 37°C for 3 hours. To dissolve the precipitation, 150 μL dimethyl sulfoxide was added per well and the absorbance of the wells was measured at a 570-nm wavelength using a microplate reader. For the colony formation assay, cells were seeded at 5×10^2 cells/500 μL/well in 24-well plates for approximately 3 days and treated with the indicated agents. After incubation at 37°C for 10 days, colonies were fixed with 4% paraformaldehyde at room temperature for 30 minutes, stained with 0.2% crystal violet for 1 hour, and washed in double-distilled water (ddH_2O). For the soft agar colony formation assay, cells were suspended at low density in top agar (0.6%) with cell culture medium containing 10% fetal bovine serum, seeded on a layer of bottom agar (1.2%), and then grown for 3 weeks.

Measurement of Intracellular ROS Levels

The level of ROS in cells was measured by a ROS Assay Kit (S0033; Beyotime), following the manufacturer's instructions. Briefly, cells were incubated with 10 μmol/L DCFH-DA (Sigma-Aldrich, Shanghai, China) in serum-free medium at 37°C for 15 minutes and then rinsed twice with PBS, followed by trypsinization and centrifugation. Then, cells were suspended in 500 μL PBS after 3 washes with PBS, and were analyzed with a BD FACS LSRII flow cytometer (BD Biosciences, San Jose, CA). Data analysis was performed with FlowJo VX software (Ashland, OR).

Cell Migration and Invasion Assays

Cell migration and invasion were performed by using 8.0-μm pore polycarbonate membrane inserts (CLS3422; Corning, Shanghai, China). A total of 1×10^5 cells in serum-free culture medium were added to the chamber, and culture medium containing 10% fetal bovine serum as a chemoattractant was added to the 24-well plate. The chamber then was incubated at 37°C for 24 hours to allow cells to

penetrate an uncoated membrane or a Matrigel-coated membrane (cat. 356234; BD Biosciences, Heidelberg, Germany). Cells remaining on the upper surface of the membrane were removed with a cotton swab, and those on the underside of the membrane were fixed with 4% paraformaldehyde and stained with 0.2% crystal violet. Migrated cells were visualized using a DM2500 fluorescence microscope (Leica, Vista, CA).

Plasmid Construction and Generation of Stable Cell Lines

For PHLDB2-Flag-tagged constructs, PHLDB2 complementary DNA (cDNA) was inserted into the pcDNA3.1 vector (Addgene) with 3× Flag at the C-terminus. For EGFR–GFP–tagged constructs, EGFR cDNA was inserted into a modified pcDNA3.1 vector containing GFP tags. For Ubiquitin (UB)-Hemagglutinin (HA)-tagged constructs, UB cDNA was inserted into modified pcDNA3.1 vector containing HA tags. Single-point and truncated mutants were generated by the Fast Mutagenesis System (FM111; Transgene, Beijing, China). For the generation of PHLDB2-overexpressed or PHLDB2-silenced CRC cells, HEK293T cells were co-transfected with pSPAX2, pMD2.G, and pCDH-CMV-MCS-EF1-Puro-PHLDB2, or shPHLDB2, or control pCDH-CMV-MCS-EF1-Puro plasmid, or control shRNA pLKO.1 plasmid. At 48 hours after transfection, lentivirus-containing medium was collected, filtered (0.45-μm filter), and supplemented with 8 mg/mL Polybrene (Sigma-Aldrich). CRC cells subsequently were transduced and selected with 2 μg/mL puromycin (540411; Calbiochem, San Diego, CA) for 2 weeks. The primer sequences are listed as follows: shPHLDB2 1: CCGGCCCTGTAGTGATGTAAGACTACTCGAGTAGTCTTACATCACTACAGGGTTTTTTG; and shPHLDB2 2: CCGGGCAGACGGCAATAATCTCTTACTCGAGTAAGAGATTATTGCCGTCTGCTTTTTTG.

RNA Extraction and Quantitative Real-Time PCR

Total RNA was extracted from the CRC lines using TRIzol reagent (15596018; Thermo Fisher Scientific), and then was reverse-transcribed using the PrimeScript RT reagent Kit with genomic DNA (gDNA) Eraser (RR047A; Takara, Beijing, China). The iTaq Universal SYBR Green Supermix (1725120; Bio-Rad, Hercules, CA) were used to quantitate the mRNA levels of the indicated genes in triplicate on a CFX Connect Real-Time PCR Detection System (Bio-Rad). The primer sequences are described as follows: PHLDB2: forward: 5'-CCTGTTGGATGTTGAAAGCA-3', reverse: 5'-GAGCCTGCTGAACAATGTGA-3'; B-myb: forward: 5'-AGCTGCACTACCAGGACACAGATT-3', reverse: 5'-TGACCTTGCACTTGCTATCCCTCT-3'; AURKA: forward: 5'-CAAAGTTTGATGAGCAGAGAACTG-3', reverse: 5'-CAGGGCATTTGCCAATTCTGTTA-3'; AURKB: forward: 5'-CTGGCCCTACGGCCGACAGA-3', reverse: 5'-CAGGCTCTTTCCGGAGGACTCG-3'; CyclinD1: forward: 5'-TATTGCGCTGCTACCGTTGA-3', reverse: 5'-CCAATAGCAGCAAACAATGTGAAA-3'; and glyceraldehyde-3-phosphate dehydrogenase: forward: 5'-AGCCACATCGCTCAGACAC-3', reverse: 5'-GCCCAATACGACCAAATCC-3'.

Gene Silencing by Small Interfering RNA

The target sequences of siMETTL14 were chemically synthesized and are shown as follows: METTL14 small interfering RNA (siRNA) 1: 5'-GCUAAAGGAUGAGUUAAU-3'; METTL14 siRNA 2: 5'-GGACUUGGGAUGAUAUUAU-3'. Negative control siRNA (small interfering scramble, siScramble) sequence was used as follows: 5'-UUCUCCGAACGUGUCACGU-3'.

RNA Sequencing Alignment and Quality Control

RNA sequencing was performed with an Illumina HiSeq 2000 (Beijing Genomics Institute, Shenzhen, Guangdong, China). A total of 20 RNA sequencing libraries were aligned with Spliced Transcripts Alignment to a Reference (STAR) software (version 2.7.4a) in 2-pass mode. First alignment pass was used to identify nonannotated junctions in the input data, allowing for the construction of a genome index containing nonannotated junctions. The second pass alignment then was performed against the junction-aware index, allowing for a more sensitive recovery of nonannotated splice junction from the data. The human genome reference used was GRCh37.p13 and GENCODE v34 (GENCODE project, https://www.gencodegenes.org/) was used as the transcriptome reference.

Quantification of Gene-Level and Transcript-Level Expression Gene Expression

Quantification was performed using RSEM (version 1.3.3, https://deweylab.github.io/RSEM/) on STAR-aligned reads. The human reference sequence and gene transfer format (GTF) file used for build RSEM index was the same as described previously, and gene expression was quantified as transcripts per million.

Differential Expression Analysis

Differential expression analysis was performed using the DESeq2 R package (https://bioconductor.org/) to compare paired primary tumor, synchronous liver metastasis, and latent liver metastasis with available gene expression data. Briefly, each patient group was categorized as a synchronous and latent group according to the timing of metastasis. Sample type was defined as primary tumor and liver metastasis, respectively. The design formula was set as type + group + type:group. Differential expressed genes were extracted using the results function (ie, type:group interaction; SL vs P, SL/P; LL vs P, LL/P; and LL vs SL, LL/SL).

Pathway Enrichment Analysis

The genes significantly expressed between SL/P, LL/P, and LL/SL (adjusted $P < .005$) were analyzed for pathway enrichment using gprofileR (https://biit.cs.ut.ee/gprofiler/gost). All statistically significant pathways from the data source Kyoto Encyclopedia of Genes and Genomes (KEGG) were obtained using a threshold of 0.05 of the g:SCS (Set Counts and Sizes) threshold.

Immunofluorescence

Cells were seeded onto the glass coverslips (WHB-24-CS; WHB Scientific, Shanghai, China) in 24-well plates. Cells were fixed with 4% paraformaldehyde in PBS for 30 minutes, permeabilized, and blocked with 0.3% Triton X-100 (T8200; Solarbio, Beijing, China) and 5% goat serum (G9023; Sigma-Aldrich) for 1 hour. After the incubation with primary antibodies at 4°C overnight, cells then were incubated further with the appropriate secondary antibodies (35552; Invitrogen for DyLight 594-conjugated goat anti-rabbit IgG, and 35511; Invitrogen for DyLight 488-conjugated goat antimouse IgG, Carlsbad, CA) for 2 hours at room temperature. Nuclei were finally stained with 4′,6-diamidino-2-phenylindole (C0060; Solarbio) for 5 minutes at a 1:5000 dilution. Fluorescence images were captured using confocal laser scanning microscopy (Carl Zeiss Microimaging, Thornwood, NY) fitted with a 63× oil immersion objective. Image analysis was performed with ImageJ software (National Institutes of Health, Bethesda, MD).

Immunohistochemistry

For immunohistochemistry (IHC), paraffin-embedded slides were deparaffinized in xylenes, followed by hydration in ethanol with gradient-decreased concentrations. Endogenous peroxidase was blocked by 3% H_2O_2. Then, the sections were boiled in antigen retrieval buffer for 3 minutes within a pressure cooker. Next, slides were incubated with the primary antibody: PHLDB2 (1:100, NBP2-38238; Novus, Littleton, CO), Ki67 (1:100, ab16667; Abcam, Cambridge, UK), or cleaved caspase-3 (1:100, 9664S; Cell Signaling Technology, Shanghai, China) at 4°C overnight, followed by treatment with MaxVision horseradish-peroxidase solution (cat. 5020; MXB Biotechnology) for 30 minutes at room temperature. After 3 washes with PBS, sections were stained with 3,3′-diaminobenzidine tetra hydrochloride peroxidase substrate (0031; MXB Biotechnology, Fuzhou, China) and counterstained with hematoxylin. Images were captured by a Pannoramic MIDI Slide scanner (3D HISTECH, Budapest, Hungary). Ki67 and cleaved caspase-3 staining was quantified by calculating positively stained cells in at least 5 randomly chosen high-power fields of each sample.

Immunoprecipitation Followed by MS

Cell lysates were prepared using IP lysis buffer (100 mmol/L NaCl, 20 mmol/L Tris-HCl, 0.5 mmol/L EDTA, pH 7.4, and 0.5% NP-40). After centrifugation to remove insoluble materials, lysates were incubated with PHLDB2 antibody at 4°C overnight. The next day, lysates were incubated with protein G–Agarose beads (16-266; Millipore) for 3 hours. The immunoprecipitated proteins were subjected to short-gel sodium dodecyl sulfate–polyacrylamide gel electrophoresis and stained for 20 minutes with Coomassie brilliant blue G-250 (175 A100615; Sangon Biotech, Shanghai, China). The protein bands of interest were excised, carefully washed, and dehydrated by acetonitrile (A955-4; Fisher Scientific). Then, 10 mmol/L dithiothreitol (D0632, Sigma-Aldrich) was applied for reduction and 55 mmol/L iodoacetamide (V900335; Sigma-Aldrich) for alkylation. Proteins were digested with trypsin (V5071; Promega, Madison, WI) for 12 hours.

After being desalted using C18 ZipTip (Millipore) according to the manufacturer's instructions, the peptide samples were loaded onto a 75 μm × 2 cm trap column and a 75 μm × 12 cm analytical column, which was packed with C18 resin (200 A, 5 μm; Michrom Bioresources, Auburn, CA) in-house. LC-MS/MS analysis was executed using an EASY-NLC 1000 nanoflow LC instrument coupled to a Q Exactive quadrupole-Orbitrap mass spectrometer (Thermo Fisher Scientific). Peptide samples were analyzed with a 65-minute gradient from 4% to 90% high-performance liquid chromatography buffer B (95% acetonitrile, 0.1% formic acid) at a flow rate of 300 nL/min. Data-dependent acquisition was performed in positive ion mode. Survey full-scan MS spectra (from m/z 350–1800) were acquired in the Orbitrap with a resolving power of 70,000 at m/z = 200. The automatic gain control value setting was set at 3e6, with maximum fill times of 20 ms. For MS/MS scans, the top 20 most intense parent ions were selected with a 1.6 m/z isolation window and fragmented with a normalized collision energy of 27%. The automatic gain control value for MS/MS was set to a target value of 1e5, with a resolution of 17,500 and a maximum fill time of 64 ms. Parent ions with a charge state of z = 1, 8, or with unassigned charge states were excluded for fragmentation. A dynamic exclusion period for the data-dependent scan was 50 seconds. All the raw files were searched against the Swiss-Prot human protein sequence database (updated in April 2019, 20,431 sequences) in Maxquant (version 1.6, https://maxquant.org). The precursor peptide mass tolerance was 10 ppm and a fragment ion mass tolerance was 0.02 daltons. Two missed trypsin cleavages were allowed. Cysteine carbamidomethylation was set as a fixed modification. Oxidation of methionine and protein N-terminal acetylation were set as variable modifications. A label-free quantification algorithm was used for protein quantification. Peptides with less than 1% false-discovery rate were chosen. A minimum of 7 unique peptides at the protein level within the full data set was required for further data processing.

Duolink In Situ Proximity Ligation Assay

Cells were seeded onto glass coverslips (WHB-24-CS; WHB Scientific) in 24-well plates, and then fixed with 4% paraformaldehyde in PBS for 30 minutes, permeabilized, and blocked with 0.3% Triton X-100 (T8200; Solarbio) and 5% goat serum (G9023; Sigma-Aldrich) for 1 hour. Cells then were incubated with mouse EGFR antibody (1:100; Santa Cruz Biotechnology) and rabbit PHLDB2 antibody (1:100, NBP2-38238; Novus) or Flag antibody (1:100, 14793S; Cell Signaling Technology) at 4°C overnight. The fluorescence signals were detected by the Duolink in situ proximity ligation assay probe (DUO92101-1KT; Sigma-Aldrich, Shanghai, China) according to the manufacturer's instructions and visualized using confocal laser scanning

microscopy (Carl Zeiss Microimaging) fitted with a 63× oil immersion objective. Image analysis was performed with ImageJ software.

Public Data Analysis

For Gene Expression Omnibus (GEO) data, the gene expression data were obtained from GSE17536 and GSE28722 as well as their corresponding clinical data using the GEO query R package. For TCGA data, the mRNA expression of each tumor was obtained from the cBioportal feature mRNA Expression, RSEM (Batch normalized from Illumina HiSeq_RNASeqV2), while survival data were obtained from the TCGA Pan-Cancer Clinical Data Resource. The mRNA expression (transcripts per million) of CRC cell lines was obtained from the Broad Institute Cancer Cell Line Encyclopedia, and cetuximab sensitivity was obtained based on published reports.[23]

Statistical Analysis

All data were analyzed by GraphPad Prism 8.0 software (San Diego, CA). Survival analysis was performed using the log-rank test. The survcutpoint function of the survminer package in R (https://cran.r-project.org/) was used to determine the optimal cut-off point based on the maximally selected log-rank statistics. The minimal proportion of observations per group was set to 30% to avoid too few patients in a certain group. Data are representative of at least 3 biologically independent experiments. Comparisons between 2 groups were performed by a 2-tailed Student *t* test. For 3 or more group analyses, the 1-way analysis of variance multiple comparison test was used. Pearson correlation and linear regression were used to determine the concordance. Data are expressed as means ± SD.

References

1. Sung H, Ferlay J, Siegel RL, Laversanne M, Soerjomataram I, Jemal A, Bray F. Global cancer statistics 2020: GLOBOCAN estimates of incidence and mortality worldwide for 36 cancers in 185 countries. CA Cancer J Clin 2021;71:209–249.
2. Pollard JW. Defining metastatic cell latency. N Engl J Med 2016;375:280–282.
3. Teng S, Li YE, Yang M, Qi R, Huang Y, Wang Q, Zhang Y, Chen S, Li S, Lin K, Cao Y, Ji Q, Gu Q, Cheng Y, Chang Z, Guo W, Wang P, Garcia-Bassets I, Lu ZJ, Wang D. Tissue-specific transcription reprogramming promotes liver metastasis of colorectal cancer. Cell Res 2020;30:34–49.
4. Malladi S, Macalinao DG, Jin X, He L, Basnet H, Zou Y, de Stanchina E, Massague J. Metastatic latency and immune evasion through autocrine inhibition of WNT. Cell 2016;165:45–60.
5. Rahbari NN, Carr PR, Jansen L, Chang-Claude J, Weitz J, Hoffmeister M, Brenner H. Time of metastasis and outcome in colorectal cancer. Ann Surg 2019;269:494–502.
6. Hanna RN, Cekic C, Sag D, Tacke R, Thomas GD, Nowyhed H, Herrley E, Rasquinha N, McArdle S, Wu R, Peluso E, Metzger D, Ichinose H, Shaked I, Chodaczek G, Biswas SK, Hedrick CC. Patrolling monocytes control tumor metastasis to the lung. Science 2015;350:985–990.
7. Quesnel B. Tumor dormancy: long-term survival in a hostile environment. Adv Exp Med Biol 2013;734:181–200.
8. Hu Z, Ding J, Ma Z, Sun R, Seoane JA, Scott Shaffer J, Suarez CJ, Berghoff AS, Cremolini C, Falcone A, Loupakis F, Birner P, Preusser M, Lenz HJ, Curtis C. Quantitative evidence for early metastatic seeding in colorectal cancer. Nat Genet 2019;51:1113–1122.
9. Chen HN, Shu Y, Liao F, et al. Genomic evolution and diverse models of systemic metastases in colorectal cancer. Gut 2021. https://doi.org/10.1136/gutjnl-2020-323703.
10. Recasens A, Munoz L. Targeting cancer cell dormancy. Trends Pharmacol Sci 2019;40:128–141.
11. Reiter JG, Makohon-Moore AP, Gerold JM, Heyde A, Attiyeh MA, Kohutek ZA, Tokheim CJ, Brown A, DeBlasio RM, Niyazov J, Zucker A, Karchin R, Kinzler KW, Iacobuzio-Donahue CA, Vogelstein B, Nowak MA. Minimal functional driver gene heterogeneity among untreated metastases. Science 2018;361:1033–1037.
12. Wiener D, Schwartz S. The epitranscriptome beyond m(6)A. Nat Rev Genet 2021;22:119–131.
13. Su R, Dong L, Li Y, Gao M, Han L, Wunderlich M, Deng X, Li H, Huang Y, Gao L, Li C, Zhao Z, Robinson S, Tan B, Qing Y, Qin X, Prince E, Xie J, Qin H, Li W, Shen C, Sun J, Kulkarni P, Weng H, Huang H, Chen Z, Zhang B, Wu X, Olsen MJ, Muschen M, Marcucci G, Salgia R, Li L, Fathi AT, Li Z, Mulloy JC, Wei M, Horne D, Chen J. Targeting FTO suppresses cancer stem cell maintenance and immune evasion. Cancer Cell 2020;38:79–96 e11.
14. Benson AB, Venook AP, Al-Hawary MM, Arain MA, Chen YJ, Ciombor KK, Cohen S, Cooper HS, Deming D, Farkas L, Garrido-Laguna I, Grem JL, Gunn A, Hecht JR, Hoffe S, Hubbard J, Hunt S, Johung KL, Kirilcuk N, Krishnamurthi S, Messersmith WA, Meyerhardt J, Miller ED, Mulcahy MF, Nurkin S, Overman MJ, Parikh A, Patel H, Pedersen K, Saltz L, Schneider C, Shibata D, Skibber JM, Sofocleous CT, Stoffel EM, Stotsky-Himelfarb E, Willett CG, Gregory KM, Gurski LA. Colon cancer, version 2.2021, NCCN Clinical Practice Guidelines in Oncology. J Natl Compr Canc Netw 2021;19:329–359.
15. Van Cutsem E, Kohne CH, Hitre E, Zaluski J, Chang Chien CR, Makhson A, D'Haens G, Pinter T, Lim R, Bodoky G, Roh JK, Folprecht G, Ruff P, Stroh C, Tejpar S, Schlichting M, Nippgen J, Rougier P. Cetuximab and chemotherapy as initial treatment for metastatic colorectal cancer. N Engl J Med 2009;360:1408–1417.
16. Xie YH, Chen YX, Fang JY. Comprehensive review of targeted therapy for colorectal cancer. Signal Transduct Target Ther 2020;5:22.
17. Woolston A, Khan K, Spain G, Barber LJ, Griffiths B, Gonzalez-Exposito R, Hornsteiner L, Punta M, Patil Y,

Newey A, Mansukhani S, Davies MN, Furness A, Sclafani F, Peckitt C, Jimenez M, Kouvelakis K, Ranftl R, Begum R, Rana I, Thomas J, Bryant A, Quezada S, Wotherspoon A, Khan N, Fotiadis N, Marafioti T, Powles T, Lise S, Calvo F, Guettler S, von Loga K, Rao S, Watkins D, Starling N, Chau I, Sadanandam A, Cunningham D, Gerlinger M. Genomic and transcriptomic determinants of therapy resistance and immune landscape evolution during anti-EGFR treatment in colorectal cancer. Cancer Cell 2019; 36:35–50 e9.

18. Bellier J, Nokin MJ, Caprasse M, Tiamiou A, Blomme A, Scheijen JL, Koopmansch B, MacKay GM, Chiavarina B, Costanza B, Rademaker G, Durieux F, Agirman F, Maloujahmoum N, Cusumano PG, Lovinfosse P, Leung HY, Lambert F, Bours V, Schalkwijk CG, Hustinx R, Peulen O, Castronovo V, Bellahcene A. Methylglyoxal scavengers resensitize KRAS-mutated colorectal tumors to cetuximab. Cell Rep 2020;30:1400–1416 e6.
19. Chong CR, Janne PA. The quest to overcome resistance to EGFR-targeted therapies in cancer. Nat Med 2013; 19:1389–1400.
20. Ye QH, Zhu WW, Zhang JB, Qin Y, Lu M, Lin GL, Guo L, Zhang B, Lin ZH, Roessler S, Forgues M, Jia HL, Lu L, Zhang XF, Lian BF, Xie L, Dong QZ, Tang ZY, Wang XW, Qin LX. GOLM1 modulates EGFR/RTK cell-surface recycling to drive hepatocellular carcinoma metastasis. Cancer Cell 2016;30:444–458.
21. Zhang KL, Zhu WW, Wang SH, Gao C, Pan JJ, Du ZG, Lu L, Jia HL, Dong QZ, Chen JH, Lu M, Qin LX. Organ-specific cholesterol metabolic aberration fuels liver metastasis of colorectal cancer. Theranostics 2021; 11:6560–6572.
22. Srinivas US, Tan BWQ, Vellayappan BA, Jeyasekharan AD. ROS and the DNA damage response in cancer. Redox Biol 2019;25:101084.
23. Lu Y, Zhao X, Liu Q, Li C, Graves-Deal R, Cao Z, Singh B, Franklin JL, Wang J, Hu H, Wei T, Yang M, Yeatman TJ, Lee E, Saito-Diaz K, Hinger S, Patton JG, Chung CH, Emmrich S, Klusmann JH, Fan D, Coffey RJ. lncRNA MIR100HG-derived miR-100 and miR-125b mediate cetuximab resistance via Wnt/beta-catenin signaling. Nat Med 2017;23:1331–1341.
24. Grimsey NJ, Coronel LJ, Cordova IC, Trejo J. Recycling and endosomal sorting of protease-activated receptor-1 is distinctly regulated by Rab11A and Rab11B proteins. J Biol Chem 2016;291:2223–2236.
25. Dittmann K, Mayer C, Kehlbach R, Rodemann HP. Radiation-induced caveolin-1 associated EGFR internalization is linked with nuclear EGFR transport and activation of DNA-PK. Mol Cancer 2008;7:69.
26. Huttlin EL, Bruckner RJ, Paulo JA, Cannon JR, Ting L, Baltier K, Colby G, Gebreab F, Gygi MP, Parzen H, Szpyt J, Tam S, Zarraga G, Pontano-Vaites L, Swarup S, White AE, Schweppe DK, Rad R, Erickson BK, Obar RA, Guruharsha KG, Li K, Artavanis-Tsakonas S, Gygi SP, Harper JW. Architecture of the human interactome defines protein communities and disease networks. Nature 2017;545:505–509.
27. Takabayashi T, Xie MJ, Takeuchi S, Kawasaki M, Yagi H, Okamoto M, Tariqur RM, Malik F, Kuroda K, Kubota C, Fujieda S, Nagano T, Sato M. LL5beta directs the translocation of filamin A and SHIP2 to sites of phosphatidylinositol 3,4,5-triphosphate (PtdIns(3,4,5)P3) accumulation, and PtdIns(3,4,5)P3 localization is mutually modified by co-recruited SHIP2. J Biol Chem 2010; 285:16155–16165.
28. Stehbens SJ, Paszek M, Pemble H, Ettinger A, Gierke S, Wittmann T. CLASPs link focal-adhesion-associated microtubule capture to localized exocytosis and adhesion site turnover. Nat Cell Biol 2014; 16:561–573.
29. Kang W, Zhang J, Huang T, Zhou Y, Wong CC, Chan RCK, Dong Y, Wu F, Zhang B, Wu WKK, Chan MWY, Cheng ASL, Yu J, Wong N, Lo KW, To KF. NOTCH3, a crucial target of miR-491-5p/miR-875-5p, promotes gastric carcinogenesis by upregulating PHLDB2 expression and activating Akt pathway. Oncogene 2021;40:1578–1594.
30. Chen G, Zhou T, Li Y, Yu Z, Sun L. p53 target miR-29c-3p suppresses colon cancer cell invasion and migration through inhibition of PHLDB2. Biochem Biophys Res Commun 2017;487:90–95.
31. Su R, Dong L, Li C, Nachtergaele S, Wunderlich M, Qing Y, Deng X, Wang Y, Weng X, Hu C, Yu M, Skibbe J, Dai Q, Zou D, Wu T, Yu K, Weng H, Huang H, Ferchen K, Qin X, Zhang B, Qi J, Sasaki AT, Plas DR, Bradner JE, Wei M, Marcucci G, Jiang X, Mulloy JC, Jin J, He C, Chen J. R-2HG exhibits anti-tumor activity by targeting FTO/m(6)A/MYC/CEBPA signaling. Cell 2018;172:90–105 e23.
32. Huang H, Weng H, Chen J. m(6)A modification in coding and non-coding RNAs: roles and therapeutic implications in cancer. Cancer Cell 2020;37:270–288.
33. Li Q, Li X, Tang H, Jiang B, Dou Y, Gorospe M, Wang W. NSUN2-mediated m5C methylation and METTL3/METTL14-mediated m6a methylation cooperatively enhance p21 translation. J Cell Biochem 2017; 118:2587–2598.
34. Tong J, Taylor P, Peterman SM, Prakash A, Moran MF. Epidermal growth factor receptor phosphorylation sites Ser991 and Tyr998 are implicated in the regulation of receptor endocytosis and phosphorylations at Ser1039 and Thr1041. Mol Cell Proteomics 2009; 8:2131–2144.
35. Biller LH, Schrag D. Diagnosis and treatment of metastatic colorectal cancer: a review. JAMA 2021; 325:669–685.
36. Recondo G, Facchinetti F, Olaussen KA, Besse B, Friboulet L. Making the first move in EGFR-driven or ALK-driven NSCLC: first-generation or next-generation TKI? Nat Rev Clin Oncol 2018;15:694–708.
37. Kumagai S, Koyama S, Nishikawa H. Antitumour immunity regulated by aberrant ERBB family signalling. Nat Rev Cancer 2021;21:181–197.
38. Goldberg RM. Cetuximab. Nat Rev Drug Discov 2005;(Suppl):S10–S11.

39. Frattini M, Saletti P, Romagnani E, Martin V, Molinari F, Ghisletta M, Camponovo A, Etienne LL, Cavalli F, Mazzucchelli L. PTEN loss of expression predicts cetuximab efficacy in metastatic colorectal cancer patients. Br J Cancer 2007;97:1139–1145.
40. Chung KY, Shia J, Kemeny NE, Shah M, Schwartz GK, Tse A, Hamilton A, Pan D, Schrag D, Schwartz L, Klimstra DS, Fridman D, Kelsen DP, Saltz LB. Cetuximab shows activity in colorectal cancer patients with tumors that do not express the epidermal growth factor receptor by immunohistochemistry. J Clin Oncol 2005; 23:1803–1810.
41. Cunningham D, Humblet Y, Siena S, Khayat D, Bleiberg H, Santoro A, Bets D, Mueser M, Harstrick A, Verslype C, Chau I, Van Cutsem E. Cetuximab monotherapy and cetuximab plus irinotecan in irinotecan-refractory metastatic colorectal cancer. N Engl J Med 2004;351:337–345.
42. Li C, Iida M, Dunn EF, Ghia AJ, Wheeler DL. Nuclear EGFR contributes to acquired resistance to cetuximab. Oncogene 2009;28:3801–3813.
43. Wheeler DL, Dunn EF, Harari PM. Understanding resistance to EGFR inhibitors-impact on future treatment strategies. Nat Rev Clin Oncol 2010;7:493–507.

Received September 7, 2021. Accepted December 10, 2021.

Correspondence
Address correspondence to: Hai-Ning Chen, MD, PhD, Department of Gastrointestinal Surgery, State Key Laboratory of Biotherapy and Cancer Center, West China Hospital, Sichuan University, Chengdu, 610041, P.R. China. Tel: +86-18980606468. e-mail: hnchen@scu.edu.cn; or Canhua Huang, PhD, State Key Laboratory of Biotherapy, West China Hospital, and West China School of Basic Medical Sciences & Forensic Medicine, Sichuan University, No. 17, Section 3, South Renmin Rd, Chengdu, 610041, P.R. China. Tel: +86-13258370346. e-mail: hcanhua@hotmail.com; fax: +86-28-85164060.

Acknowledgments
The authors would like to thank Ping Fan of West China Biobanks, Department of Clinical Research, West China Hospital of Sichuan University for biospecimen collection, processing, quality control, and storage.

Ethics Approval
This study was approved by the Ethics Committee of West China Hospital, Sichuan University (2019 [338]; 2020 [374]). The study was performed in accordance with the Declaration of Helsinki.

Data Availability Statement
Further information and requests for resources and reagents should be directed to and will be fulfilled by the Lead Contact, Hai-Ning Chen (hnchen@scu.edu.cn). Most data supporting the findings of this study are available within the article and online supplementary files. The raw sequencing data from this study have been deposited in the Genome Sequence Archive in BIG Data Center, Beijing Institute of Genomics, Chinese Academy of Sciences, under accession number PRJCA007055 (BioProject), which can be accessed at http://bigd.big.ac.cn/gsa-human. All other data are available from the corresponding author upon reasonable request.

CRediT Authorship Contributions
Hai-Ning Chen, PhD, MD (Conceptualization: Lead; Supervision: Equal; Writing – review & editing: Equal)
Maochao Luo (Conceptualization: Supporting; Investigation: Equal; Writing – original draft: Lead)
Zhao Huang (Conceptualization: Supporting; Investigation: Equal)
Xingyue Yang (Investigation: Equal; Writing – original draft: Equal)
Yan Chen (Investigation: Equal)
Jingwen Jiang (Investigation: Supporting)
Lu Zhang (Investigation: Supporting)
Li Zhou (Investigation: Supporting)
Siyuan Qin (Investigation: Supporting)
Ping Jin (Investigation: Supporting)
Shuyue Fu (Investigation: Supporting)
Liyuan Peng (Investigation: Supporting)
Bowen Li (Investigation: Supporting)
Yongting Fang (Investigation: Supporting)
Wenchen Pu (Methodology: Supporting)
Yanqiu Gong (Methodology: Supporting)
Yu Liu (Methodology: Supporting)
Zhixiang Ren (Formal analysis: Supporting)
Qiu-Luo Liu (Investigation: Supporting)
Cun Wang (Resources: Supporting)
Fangqiong Xiao (Resources: Supporting)
Du He (Resources: Supporting)
Hongying Zhang (Resources: Supporting)
Changlong Li (Resources: Supporting)
Heng Xu (Funding acquisition: Supporting; Resources: Supporting)
Lunzhi Dai (Methodology: Supporting)
Yong Peng (Writing – review & editing: Supporting)
Zong-Gung Zhou (Funding acquisition: Supporting; Resources: Equal)
Canhua Huang (Conceptualization: Equal; Funding acquisition: Lead; Supervision: Equal; Writing – review & editing: Supporting)

Conflicts of interest
The authors disclose no conflicts.

Funding
This work was supported by grants from the National Key Research and Development Project of China (2020YFA0509400 and 2020YFC2002705), the national natural science foundation of china (81702378, 82073246, 81821002, 81790251, 82130082, and 82003098), Guangdong Basic and Applied Basic Research Foundation (2019B030302012), Sichuan Science and Technology Program (22CXRC0248, 2020YJ0105, and 2020YJ0094), and the 1.3.5 project for disciplines of excellence, West China Hospital, Sichuan University (2016105, ZYGD20006, and ZYYC20003).